

# Chlorine oxidation of VOCs at a semi-rural site in Beijing: Significant chlorine liberation from ClNO<sub>2</sub> and subsequent gas and particle phase Cl-VOC production

Michael Le Breton<sup>1</sup>, Åsa M Hallquist<sup>2</sup>, Ravi Kant Pathak<sup>1</sup>, David Simpson<sup>3,4</sup>, Yujue Wang<sup>5</sup>, John Johansson<sup>3</sup>, Jing Zheng<sup>5</sup>, Yudong Yang<sup>5</sup>, Dongjie Shang<sup>5</sup>, Haichao Wang<sup>5</sup>, Qianyun Liu<sup>6</sup>, Chak Chan<sup>7</sup>, Tao Wang<sup>8</sup>, Thomas J. Bannan<sup>9</sup>, Michael Priestley<sup>9</sup>, Carl J Percival<sup>9\*</sup>, Dudley E Shallcross<sup>10</sup>, Keding Lu<sup>5</sup>, Song Guo<sup>5</sup>, Min Hu<sup>5</sup> and Mattias Hallquist<sup>1</sup>

<sup>1</sup>Department of Chemistry and Molecular Biology, University of Gothenburg, Gothenburg, Sweden

<sup>2</sup>IVL Swedish Environmental Research Institute, Gothenburg, Sweden

<sup>3</sup>Earth and Space Sciences, Chalmers University of Technology, Gothenburg, Sweden

<sup>4</sup>Norwegian Meteorological Institute, Oslo, Norway

<sup>5</sup>State Key Joint Laboratory of Environmental Simulation and Pollution Control, College of Environmental Sciences and Engineering, Peking University, Beijing, China

<sup>6</sup>Division of Environment and Sustainability, The Hong Kong University of Science and Technology, Clearwater Bay, Kowloon, Hong Kong

<sup>7</sup>School of Energy and Environment, City University of Hong Kong, Hong Kong

<sup>8</sup>Department of Civil and Environmental Engineering, The Hong Kong Polytechnic University, Hong Kong, China

<sup>9</sup>Centre for Atmospheric Science, School of Earth, Atmospheric and Environmental Science, University of Manchester, Manchester, UK

<sup>10</sup>School of Chemistry, University of Bristol, Cantock's Close, Bristol, BS8 1TS, UK

\* Now at Jet Propulsion laboratory, Pasadena, California, USA.

Correspondence to: M. le Breton (Michael.le.breton@gu.se)

**Abstract.** Nitryl Chloride (ClNO<sub>2</sub>) accumulation at night-time acts as a significant reservoir for active chlorine and impacts the following day's photochemistry when the chlorine atom is liberated at sunrise. Here, we report simultaneous measurements of N<sub>2</sub>O<sub>5</sub> and a suite of inorganic halogens including ClNO<sub>2</sub> and Cl-VOCs in the gas and particle phase utilizing the FIGAERO-ToF-CIMS during an intensive measurement campaign 40 km Northwest of Beijing in May and June 2016. A maximum mixing ratio of 2900 pptV of ClNO<sub>2</sub> was observed with a mean campaign night-time mixing ratio of 487 ppt, appearing to have an anthropogenic source supported by correlation with SO<sub>2</sub>, CO and benzene, which often persisted at high levels after sunrise until midday. This was attributed to such high mixing ratios persisting after numerous e-folding times of the photolytic lifetime enabling the chlorine atom production to reach 2.3 x 10<sup>5</sup> molecules cm<sup>-3</sup> from ClNO<sub>2</sub> alone, peaking at 9:30 am and up to 8.4 x 10<sup>5</sup> molecules cm<sup>-3</sup> when including the supporting inorganic halogen measurements.

Cl-VOCs were measured in the particle and gas phase for the first time at high time resolution and illustrate how the iodide ToF-CIMS can detect unique markers of chlorine atom chemistry in ambient air from both biogenic and anthropogenic sources. Their presence and abundance can be explained via time series of their measured and steady state calculated precursors, enabling the assessment of competing OH and chlorine atom oxidation via measurements of products from both of these mechanisms and their relative contribution to SOA formation.



1 constants with a number of VOCs 200 times larger than OH (Tanaka *et al.*, 2003); therefore, its abundance, fate  
2 and cycling can significantly alter standard daytime oxidation pathways. The oxidation of VOCs by chlorine atoms  
3 is thought to be significant in the early hours of the day while OH mixing ratios are low and chlorine atom  
4 production is high through the photolysis of ClNO<sub>2</sub>, as well as feeding into the standard HO<sub>x</sub>/NO<sub>x</sub> cycles via  
5 production of peroxy radicals from reactions with alkanes. Additional Cl<sub>2</sub> photolysis and HCl reaction with OH  
6 can also produce chlorine atoms throughout the day but at lower rates.

7 The oxidation mechanism of saturated hydrocarbon (R12-R13) is initiated by reaction with OH or chlorine atom  
8 to form an organic peroxy radical (RO<sub>2</sub>), and H<sub>2</sub>O or HCl depending on the oxidant, which is the dominant pathway  
9 for chloride-VOC reactions. In a heavily polluted environment such as Beijing, the RO<sub>2</sub> favours further reactions  
10 with NO to form an oxygenated volatile organic compound, HO<sub>2</sub> and NO<sub>2</sub> or an alkyl nitrate RONO<sub>2</sub>. Specifically,  
11 acyl peroxy radicals can also react with NO<sub>2</sub> to form acyl peroxy nitrates (APN) such as peroxy acetyl nitrate  
12 (PAN).



18 Addition of the chlorine atom to unsaturated VOC can also occur and then continue on the similar reaction pathway  
19 as R12 – R15. These pathways result in the production of unique chlorine atom chemistry markers which have  
20 been previously investigated to indicate the extent of chlorine atom oxidation reactions (Riemer *et al.*, 2008, Keil  
21 and Shepson, 2006). The utilization of these compounds, such as 2-chloroperoxypropionyl nitrate (2-Cl PPN) and  
22 1-chloro-3-methyl-3butene-2-one (CMBO) as chlorine atom chemistry markers relies on the abundance of the  
23 chlorine atom, the VOC precursor; HO<sub>x</sub>, NO<sub>x</sub> and O<sub>3</sub> and competing pathways for chlorine atom reactions. Riedel  
24 *et al.* (2014) calculated that up to tens of ppt Cl-VOCs are formed as a result of chlorine atom addition to alkenes  
25 and can therefore provide a number of potential periods of dominating active Cl chemistry (Wang *et al.*, 2001).

26 The production of chloroperoxy radicals via chlorine atom addition can lead to the formation of semi volatile  
27 oxidation products which have been observed for both biogenic (Cai and Griffin *et al.*, 2006) and anthropogenic  
28 emissions (Huang *et al.*, 2014, Riva *et al.*, 2015) in controlled laboratory studies. Chlorine initiated oxidation of  
29 isoprene could also represent a significant oxidation pathway due to its rapid reaction rate compared to OH  
30 (Orlando *et al.*, 2003) resulting in gas phase products such as chloroacetaldehyde and CMBO, a unique tracer for  
31 atmospheric chlorine atom chemistry (Nordmeyer *et al.*, 1997). Furthermore, reactions of the chlorine atom with  
32 isoprene or its SOA derived products could serve as an atmospheric chlorine sink (Ofner *et al.*, 2012). Wang *et al.*  
33 (2017) revealed chlorine initiated oxidation of isoprene can produce SOA yields up to 36%, with products similar  
34 to that of OH isoprene oxidation, compared to the 15% yield from standard oxidation calculated by Liu *et al.*  
35 (2016), although this is known to be a factor of 2 higher than utilised in standard climate models. This SOA

1 formation from chlorine initiated oxidation presents a large knowledge gap in the literature, which to date is limited  
2 by measurement capabilities.

3 This complex system results in a large uncertainty in the global budget of chlorine atoms  $\sim 15\text{--}40 \text{ Tg Cl yr}^{-1}$   
4 calculated by indirect means (Allan *et al.*, 2007; Platt *et al.*, 2004), which is further limited by the ability of  
5 measurement techniques to accurately quantify short lived species at low mixing ratios. Our knowledge of the Cl  
6 budget therefore depends on the accurate measurement of its precursors, namely ClNO<sub>2</sub> and major reaction  
7 pathways of the chlorine atom upon liberation in the daytime. Measurements to date show that the mixing ratio of  
8 ClNO<sub>2</sub> vary geographically from below limits of detection to hundreds of ppt (Mielke *et al.*, 2015, Phillips *et al.*,  
9 2012, Bannan *et al.*, 2015) and up to 3 ppb (Tham *et al.*, 2014, Riedel *et al.* 2014, Liu *et al.*, 2017) in heavily  
10 polluted urban areas. To date, the majority of these measurements have been performed in the United States,  
11 although research globally and in China have recently been published (Tham *et al.*, 2014, T Wang *et al.*, 2016, X.  
12 Wang *et al.*, 2017, Z. Wang, Liu *et al.* 2017).

13 Iodide adduct ionization has previously been applied to measure inorganic halogens in ambient air (Osthoff *et al.*,  
14 2008, Riedel *et al.*, 2012, Thornton *et al.*, 2010, Le Breton *et al.*, 2017a) using mass spectrometers with quadrupole  
15 mass analysers. This technique involves periodically changing the tuning of the spectrometer to allow transmission  
16 of a particular mass ion to the detector. Several species are therefore often “chosen” for detection in order to  
17 achieve high enough time resolution. Recent developments and availabilities of a Time of Flight Chemical  
18 Ionisation Mass Spectrometer (ToF-CIMS) have enabled the simultaneous measurement of all detectable ions by  
19 an ionization technique via high frequency full mass spectral collection. The high resolving power (3500) of this  
20 technique also enables much lower limits of detection for species which may have the similar mass to a compound  
21 that is much more abundant via multi peak fitting. This technique has previously been applied for the measurement  
22 of ClNO<sub>2</sub> and Cl<sub>2</sub> (Faxon *et al.* 2015) and recently for Cl-VOCs (Wang *et al.*, 2017) in the gas phase. In this study,  
23 a ToF-CIMS utilizing the FIGAERO (Filter Inlet for Gas and AEROsols) is deployed at a site in semi-rural Beijing,  
24 China to measure the gas and particle phase precursor (ClNO<sub>2</sub>, N<sub>2</sub>O<sub>5</sub>) and selective halogen containing species at  
25 high time frequency and resolving power to further our understanding of the chlorine atom budget in this region  
26 and its potential fate.

27

## 28 **2. Experimental**

### 29 **2.1 Site description**

30 The data presented here was collected during the inter-collaborative field campaign, within the framework of a  
31 Sino-Sweden research project “Photochemical Smog in China” aimed to further our understanding of the episodic  
32 pollution events in China through gas and particle phase measurements with numerous analytical instruments. The  
33 laboratory setup in the Changping University Campus of PKU was situated at a semi-rural site 40 km North West  
34 of Beijing close to Changping town (40.2207° N, 116.2312° E). The general setup has previously been described  
35 by Le Breton *et al.*, 2017b.

36

1 All instruments sampled from inlets setup in a laboratory 12 metres high from the 13<sup>th</sup> May 2016 to 23<sup>rd</sup> June 2016.  
2 The site has a small town within its vicinity and some small factories within 5 kilometers. A High Resolution Time  
3 of Flight Aerosol Mass Spectrometer (HR-ToF-AMS) was utilized to measure the mass mixing ratios and size  
4 distributions of non-refractory species in submicron aerosols, including organics, sulfate, ammonium and chloride  
5 (DeCarlo *et al.*, 2006, Hu *et al.*, 2013). The setup of this instrument has been previously described by Hu *et al.*,  
6 (2016). Photolysis rates were measured by a spectroradiometer for O<sub>3</sub>, NO<sub>2</sub>, HCHO, HONO and H<sub>2</sub>O<sub>2</sub>. The  
7 photolysis rate of any given species was calculated by normalizing to the cross section and quantum yields taken  
8 from the recommendations of the Jet Propulsion Laboratory (JPL) kinetic evaluation report (Burkholder *et al.*,  
9 2015).

10 An Ionicon Analytik high sensitivity PTR-MS (Proton TRansfer Mass Spectrometer) as described by de Gouw  
11 and Warneke *et al.*, (2007) provided supporting precursor VOC measurements. Detailed information about the PTR  
12 MS measurements can be found in Yuan *et al.* 2012 and 2013. In brief, 28 masses are measured for the campaign  
13 at 1 Hz. Zero air, which was produced by ambient air passing through a platinum catalytic converter at 350 °C  
14 (Shimadzu Inc., Japan), was measured for 15 min every 2.5 hours to determine the background. used to measure  
15 background Aromatics masses (m/z 79 for benzene, m/z 93 for toluene, m/z 105 for styrene, m/z 107 for C8  
16 aromatics and m/z 121 for C9 aromatics), oxygenated masses (m/z 33 for methanol, m/z 45 for acetaldehyde, m/z  
17 59 for acetone, m/z 71 for MVK+MACR and m/z 73 for MEK), isoprene (m/z 69) and acetonitrile (m/z 42) were  
18 calibrated by using EPA TO15 standard from Apel-Riemer Environmental Inc., USA. Formic acid (m/z 47), acetic  
19 acid (m/z 61), formaldehyde (m/z 31), and monoterpenes (m/z 81 and m/z 137) were calibrated by permeation  
20 tubes (VICI, USA).

21

## 22 **2.2 ToF-CIMS setup**

23 Gas and particle phase ambient species were measured using an iodide ToF-CIMS (resolving power of 3500)  
24 coupled to the FIGAERO inlet (Lopez-Hilfiker *et al.*, 2014). The setup for this campaign has previously been  
25 described by le Breton *et al.* (2017b). Briefly, the iodide ionization scheme was utilised to acquire non-fragmented  
26 ions of interest by passing UHP N<sub>2</sub> over a permeation tube containing liquid CH<sub>3</sub>I (Alfa Aesar, 99%), and through  
27 a Tofwerk X-Ray Ion Source type P (operated at 9.5 kV and 150 μA) to produce the iodide reagent ions. The  
28 ionized gas was then carried out of the ion source and into the Ion-Molecule Reaction (IMR) chamber, which was  
29 heated to 40 degrees Celsius to reduce wall loss, through an orifice (Ø = 1 μm). The inlet lines were 2 metres long  
30 and composed of copper tubing (12 mm) for the aerosol inlet and Teflon tubing (12 mm) for the gas sample line.  
31 Particles were collected onto a Zefluor® PTFE membrane filter at the same rate as the gas inlet line sampling, 2  
32 SLM. The FIGAERO was operated in a cyclic pattern; 25 minutes of gas phase measurement and simultaneous  
33 particle collection, followed by a 20 minute period during which the filter was shifted into position over the IMR  
34 inlet and the collected particle mass was desorbed.

35

## 36 **2.3 Calibration**

37 In the field formic acid calibrations were performed daily utilising a permeation source maintained at 40 °C. A dry  
38 N<sub>2</sub> flow (200 sccm) was passed over the permeation source and joined a 2 SLM N<sub>2</sub> flow line directed towards the

1 inlet. The mixing ratio of the flow was determined by mass loss in the laboratory after the campaign. The sensitivity  
2 of the ToF-CIMS to formic acid was found to be 3.4 ion counts per ppt Hz<sup>-1</sup> for 1x10<sup>5</sup> iodide ion counts.

3 N<sub>2</sub>O<sub>5</sub> was synthesized by mixing 20 ppm O<sub>3</sub> with pure NO<sub>2</sub> (98%, AGA Gas) in a glass vessel and then passing  
4 the mixture through a cold trap held at -78.5 °C by dry ice. The N<sub>2</sub>O<sub>5</sub> was transferred to a diffusion vial fitted with  
5 a capillary tube (i.d. 2 mm). The N<sub>2</sub>O<sub>5</sub> diffusion source was held at a constant temperature (-23 °C), and the mass  
6 loss rate was characterized gravimetrically for a flow rate of 100 sccm. The same flow was added to a dry nitrogen  
7 inlet dilution flow of 2 SLM to calibrate the CIMS. ClNO<sub>2</sub> measurements were quantified by passing the N<sub>2</sub>O<sub>5</sub>  
8 over a wetted NaCl bed to produce ClNO<sub>2</sub>. The decrease in N<sub>2</sub>O<sub>5</sub> from the reaction with NaCl was assumed to be  
9 equal to the mixing ratio of ClNO<sub>2</sub> produced (i.e., a 100% yield). Conversion of N<sub>2</sub>O<sub>5</sub> to ClNO<sub>2</sub> can be as efficient  
10 as 100% on sea salt, but it can also be lower, for example if ClNO<sub>2</sub> were to convert to Cl<sub>2</sub> (Roberts et al., 2008).  
11 For NaCl the conversion efficiency has however been as low as 60% (Hoffman et al., 2003). In this calibration we  
12 have followed the accepted methods of Osthoff et al., (2008) and Kercher et al., (2009) that show a conversion  
13 yield of 100% and have assumed this yield in the calibrations of this study. The lower detection limit of the CIMS  
14 to N<sub>2</sub>O<sub>5</sub> and ClNO<sub>2</sub> was found to be 9.5 and 1.2 ppt respectively for 1 minute averaged data. Using the error in  
15 the individual slope of the calibrations results in a total uncertainty of 30% for both N<sub>2</sub>O<sub>5</sub> and ClNO<sub>2</sub>. These  
16 sensitivities for N<sub>2</sub>O<sub>5</sub> and ClNO<sub>2</sub> (9.8 and 1.6 ion counts per ppt Hz<sup>-1</sup> for 1x10<sup>5</sup> iodide ion counts) were applied  
17 relatively to that of formic acid. The other inorganic halogens reported in this work are assumed to have the same  
18 sensitivity as ClNO<sub>2</sub>. This is in line with that Le Breton et al. (2017) reported many inorganic halogens possess a  
19 similar, if not the same, sensitivity, which is also supported by our chloroacetic acid calibration. Other acids  
20 identified by CIMS which are reported in the literature are given the sensitivity of N<sub>2</sub>O<sub>5</sub> to provide a minimum  
21 concentration so no concentrations are over estimated.

22 A post campaign calibration of chloroacetic acid (99%, Sigma Aldrich) was utilised to apply a sensitivity factor  
23 for all Cl-VOCs measured during the campaign. The calibration was performed using the same method as for  
24 formic acid and gave a sensitivity of 1.02 ion counts ppt<sup>-1</sup> Hz when normalized to 1x10<sup>5</sup> I<sup>-</sup> ion counts. Using  
25 relative sensitivities will increase the uncertainties, but is a commonly applied method within the CIMS  
26 community, although in this specific case it is very likely that the sensitivity is similar for all inorganic/organic  
27 halogens, as demonstrated by Le Breton et al. (2017a).

28

## 29 **2.4 Model setup**

30 The EMEP MSC-W chemical transport model (Simpson et al., 2012, Simpson et al., 2017) driven by meteorology  
31 from the WRF-ARW model (Skamarock et al., 2008) was utilised to support source analysis of the particulate  
32 chloride. The model was run on two nested domains (0.5° and 0.1667° resolution respectively) with biomass  
33 burning emissions from the two databases FINN and GFAS, and anthropogenic emissions from the MEIC  
34 inventory (<http://meicmodel.org/>). Two versions of the model, one getting emissions from open biomass burning  
35 from the Fire Inventory from NCAR (FINN) (Wiedinmyer et al., 2011) and one getting them from the Global Fire  
36 Assimilation System (GFAS) (Kaiser et al., 2012), were run for the entire period of the Changping measurement  
37 campaign.

## 1 **Results and Discussion**

### 2 **3.1 Peak identification and quantification**

3 Peak fitting was performed utilizing the Tofware peak fitting software for molecular weights up to 620 AMU. The  
4 standard peak shape was fitted a peak on the spectra until the residual was less than 5%. Each unknown peak was  
5 assigned a chemical formula using the peaks exact mass maxima to 5 decimal places and also isotopic ratios of  
6 subsequent minor peaks. An accurate fitting was characterized by a ppm error of less than 5 and subsequent  
7 accurate fitting of isotopic peaks. The analysis here focuses on species identified in the mass spectra considered to  
8 possibly play important roles with respect to the night-time chlorine reservoir and several other key night-time  
9 oxidants; ClNO<sub>2</sub>, HCl, Cl<sub>2</sub>, ClO, HOCl, OClO, ClONO<sub>2</sub>, N<sub>2</sub>O<sub>5</sub> and Cl-VOCs. Figure 1 displays the average mass  
10 spectra for the measurement campaign and the peak fitting applied for ClO and ClNO<sub>2</sub>. All species were a dominant  
11 peak with a multi peak fit, although a number of co-existing peaks were present for much of the campaign. This  
12 signifies the importance of high resolution fit data and the need for high resolution measurements. A quadrupole  
13 CIMS may not be able to resolve the peak adjacent to ClO at m/z 178 (dominant peak is IC<sub>6</sub>F<sub>3</sub>HO<sub>3</sub><sup>-</sup>) and the second  
14 dominant peak for the ClNO<sub>2</sub> fit (cluster of HNO<sub>3</sub> with water) would result in a 10% over estimation.

15

### 16 **3.2 N<sub>2</sub>O<sub>5</sub> measurements**

17 The CIMS and a Cavity Enhanced Absorption Spectrometer (CEAS) measured N<sub>2</sub>O<sub>5</sub> (Wang *et al.*, 2017)  
18 simultaneously from the 13<sup>th</sup> May 2016 to the 6<sup>th</sup> June 2016. However, given the use of the FIGAERO, the CIMS  
19 alternated measurements between gas and particle phases so did not generate a completely continuous gas phase  
20 time series. Here, the CEAS is utilised to validate the CIMS N<sub>2</sub>O<sub>5</sub> (at m/z 235) measurements and also instrument  
21 stability. The CEAS utilised a dynamic source by mixing NO<sub>2</sub> and O<sub>3</sub> to generate stable N<sub>2</sub>O<sub>5</sub> for calibration (Wang  
22 *et al.*, 2017). The source was used to calibrate the ambient sampling loss of N<sub>2</sub>O<sub>5</sub> in the sampling line, filter, the  
23 preheater cavity and optical cavity. This was performed pre and post campaign. During the campaign the  
24 reflectivity of the high reflectivity mirror was calibrated daily and filter changed hourly. The simultaneous  
25 measurements of N<sub>2</sub>O<sub>5</sub> can be shown in Figure 2 for one minute averaged data. The time series show a good  
26 agreement for both background mixing ratios during the day (sub 10 ppt) and high night-time mixing ratios (up to  
27 800 ppt), excluding one night. The highest N<sub>2</sub>O<sub>5</sub> levels observed by both the CEAS and CIMS were observed on  
28 the 3<sup>rd</sup> June although the CEAS reports 880 ppt whereas the CIMS reports 580 ppt. If included in the analysis the  
29 R<sup>2</sup> is 0.71 and when excluded it is 0.76. To date the reason for this deviation during that night is not known but it  
30 should be stressed that N<sub>2</sub>O<sub>5</sub> measurements are delicate and highly depending on sampling condition, e.g. the RH.  
31 Nevertheless, excluding this night from the comparison, a slope of 0.85 is observed and a y offset of 0.9 ppt. The  
32 diurnal profile in Figure 2 represented the difference between the two measurements throughout the campaign.  
33 The largest error between the two measurements occurs at night during the higher levels of N<sub>2</sub>O<sub>5</sub>, although  
34 averaging at 4 ppt (representing 11% error on the average campaign concentration). Differences could arise from  
35 a number of various factors. Inlet differences such as the CIMS heated IMR (to 40 °C to reduce wall loss), residence  
36 time and ambient NO<sub>2</sub> can all change thermal decomposition and wall loss rates between the instruments, which  
37 is determined for the CEAS in Wang *et al.* (2017) but not for the CIMS in this work. Also, the separate inlets were

1 facing in different directions within the same laboratory, possibly enabling local wind patterns to affect the mixing  
2 ratios reaching each instrument.

3 The CEAS data was further utilised to assess any sensitivity changes for the CIMS that daily carboxylic acid  
4 calibrations did not account for. A time series of hourly factor differences between the CIMS and CEAS was  
5 implemented into the data to weight the measurements to a normalised sensitivity. The high level of agreement  
6 from low mixing ratio measurements and a species with a short lifetime from different inlets confirms the accuracy  
7 and reliability of the CIMS measurements for this campaign.

8 Generally,  $N_2O_5$  was detected throughout the campaign with a clear diurnal variation peaking at night-time and  
9 rapidly falling to below limits of detection in the daytime as a result of photolysis of  $N_2O_5$  and  $NO_3$ . The campaign  
10 mean night-time mixing ratio was 121 ppt with a standard deviation of 76 ppt. The maximum mixing ratio of  $N_2O_5$   
11 observed was 880 ppt on the 3<sup>rd</sup> June. This range of mixing ratios lie within the recently reported values in the  
12 literature, but not at the extreme mixing ratios as observed in Germany (2.5 ppb) (Phillips *et al.*, 2016) or Hong  
13 Kong (7.7 ppb) by Wang *et al.* (2016) and Brown *et al.* (2017). Although the mean mixing ratios do not increase  
14 significantly during the pollution episodes, the maximum mixing ratios detected overnight increase by up to a  
15 factor of 4.

16

### 17 **3.3 Inorganic chlorine: Abundance, profiles and source**

#### 18 **3.3.1 Abundance and profiles**

19 Mean diurnal profiles of HCl, Cl<sub>2</sub>, ClONO<sub>2</sub>, HOCl, ClO and ClNO<sub>2</sub> are displayed in Figure 3 from data between  
20 the 23<sup>rd</sup> May and the 6<sup>th</sup> June. HCl exhibited a standard diurnal profile increasing in mixing ratio throughout the  
21 day and peaking at 4 pm which then fell off slowly at night. The mean HCl campaign mixing ratio was 510 ppt  
22 (standard deviation ( $\sigma$ ) 270 ppt) and the maximum HCl mixing ratio was 1360 ppt on the 30<sup>th</sup> June. Cl<sub>2</sub> exhibited  
23 a diurnal profile peaking at both the night-time and daytime. High mixing ratios were observed at night followed  
24 by a sharp loss at sunrise and a general build-up throughout the day. The campaign mean mixing ratio was 0.65  
25 ppt ( $\sigma$  0.5 ppt) and the maximum mixing ratio was 4.2 ppt on the 4<sup>th</sup> June just before midnight. This agrees well  
26 with recent urban measurements of Cl<sub>2</sub> in the USA where Faxon *et al.* (2015) observed a maximum of 3.5 ppt and  
27 Finley *et al.* (2006) observed up to 20 ppt in California. Up to 500 ppt Cl<sub>2</sub> has recently been reported in the Wangdu  
28 County, South West of Beijing (Liu *et al.*, 2017). Although the mixing ratios we report here are significantly lower,  
29 as detailed later, their source maybe of similar origin, which is indicated to be from power plant emissions.

30 The diurnal profile of HOCl peaked during the daytime via its main formation pathways are via reaction of ClO  
31 and HO<sub>2</sub> and Cl with OH. Interestingly the ClO in this work exhibits a night-time diurnal peak, contradicting  
32 known formation pathways via Cl reaction with O<sub>3</sub> and the photolysis of ClONO<sub>2</sub>. The complexity continues as  
33 ClONO<sub>2</sub> also peaks during the night, given that its main known formation pathway is via reaction of ClO  
34 (produced at sunrise via ClNO<sub>2</sub> photolysis) with NO<sub>2</sub>. The misidentification of ClONO<sub>2</sub> and ClO is not thought  
35 to be a possible reason for these discrepancies due to the low number of mass spectral peaks that have maxima at  
36 night and the mass defect of chlorine making the peak position unique to chlorine containing molecules. IMR



1 chemistry is also not a possible source as these reactions would occur throughout the day, therefore skewing all of  
2 the data and not just the night-time levels, although there is a possibility that ClONO<sub>2</sub> can be formed in the IMR  
3 by reactions between ClO and NO<sub>2</sub>. It is hypothesized that in extremely high OH and HO<sub>2</sub> mixing ratios, all ClO  
4 is rapidly converted to HOCl, limiting the formation on significant levels of ClO and subsequently ClONO<sub>2</sub>. Khan  
5 et al (2008) suggest that Cl atoms of around 2x10<sup>4</sup> molecules cm<sup>-3</sup> could be present at night via analysis of alkane  
6 relative abundance. Although a formation mechanism is not proposed, it provides further evidence that ClO  
7 formation at night-time is possible and may represent an unknown reaction pathway, which would agree with the  
8 measurements presented in this work.

9 ClONO<sub>2</sub> exhibited a similar diurnal profile as N<sub>2</sub>O<sub>5</sub>, peaking at night-time and lost during daylight due to  
10 photolysis. The campaign mean night-time mixing ratio was 487 ppt. The maximum mixing ratio observed was  
11 2900 ppt on the 31st May, similar to that previously measured at semi-rural site in Wangdu (up to 1500 ppt) (Liu  
12 et al., 2017), Mount Tai (2000 ppt) (Wang et al., 2017), but lower than that in Hong Kong (4 ppb) (Wang et al  
13 2016).

14

### 15 **3.3.2 Source of chloride**

16 The high levels of ClONO<sub>2</sub> indicate a local significant source of chlorine to support these observations. The  
17 dominant source of chlorine atoms for ClONO<sub>2</sub> production within models, such as the Master Chemical Mechanism  
18 (MCM), is from sea salt. However, the site is situated 200 km from the Yellow Sea and therefore this origin would  
19 have a low probability. The mean AMS chloride mass loading was 0.05 µg m<sup>-3</sup> for the campaign with a maximum  
20 of 1.7 µg m<sup>-3</sup>. The Cl<sup>-</sup> from the AMS appears to be correlated strongly with CO and SO<sub>2</sub>, possibly originating  
21 from power plants or combustion sources. It should be noted that the AMS data does not include refractory aerosol  
22 and also has a cut off size larger than anticipate size of sea salt particles. Instead, the high Cl<sup>-</sup> observed appears to  
23 originate from mainland areas to the site (Figure 4) rather from the nearest coast, further supporting a strong  
24 anthropogenic source. Tham et al., (2016) observed a strong correlation of aerosol chloride with SO<sub>2</sub> and  
25 potassium from measurements done during the same season in 2014 at Wangdu (semi-rural site 160 km south  
26 West of Beijing) and suggested contribution to fine chloride from burning of coal and crop residues. The latter  
27 was also supported by satellite fire spot count data (Tham et al., 2016). Riedel et al. (2013) have previously reported  
28 high ClONO<sub>2</sub> mixing ratios observed from urban and power plant plumes measuring high mixing ratios of gas phase  
29 Cl<sub>2</sub>. The correlation with SO<sub>2</sub> indicates coal burning as a potential source of particulate chlorine which is known  
30 to be a significant source of PM in the Beijing region (Ma et al., 2017), and the correlation with CO and benzene  
31 could be an indicator of biomass burning (Wang et al., 2002). To support this analysis, figure S1 displays a wind  
32 rose plot in which radial and tangential axes represent the wind direction and speed (km h<sup>-1</sup>). The colour bar  
33 represents the PM<sub>2.5</sub> concentration. We could see that during the campaign, the severe pollution was from the  
34 south and southwest, with little contribution from the east part. Therefore, we could deduce that little contribution  
35 of the chloride was from the ocean.

36 In order to test the hypothesis of biomass burning as a source of particulate chlorine, biomass burning emissions  
37 and transport utilising the EMEP MSC-W chemical transport model driven by meteorology from the WRF-ARW  
38 model (Skamarock et al., 2008) were used. Neither of the two biomass burning databases used (FINN and GFAS)

1 contained data on chlorine emissions, so instead the biomass burning emissions of CO (CO<sub>bb</sub>) were tracked and  
2 compared to the total mixing ratio of CO (CO<sub>t</sub>) at the Changping site. CO was chosen since the measurements at  
3 Changping had shown strong correlation between CO and ClNO<sub>2</sub> and because CO could be expected to be co-  
4 emitted with chlorine for both biomass burning and industrial combustion.

5 Figure S2 (supplementary) shows time series of the measured ClNO<sub>2</sub> mixing ratios at the Changping site, as well  
6 as the modelled mixing ratios of CO<sub>t</sub> and CO<sub>bb</sub>. CO<sub>bb</sub> is shown for calculations using either the FINN or the  
7 GFAS data base, while for clarity the CO<sub>t</sub> is only shown using the FINN data base. From this figure it is clear that  
8 mixing ratios of CO<sub>bb</sub> are very low compared to CO<sub>t</sub>. The two pollution episodes on May 18-May 23 and May  
9 28-June 5, are to some extent visible in all time series, but for the biomass burning CO series, the second episode  
10 is much less pronounced. Night-time averages of the mixing ratios shown in figure S2 were calculated for each  
11 night for the time period 18:00 to 08:00 local time (UTC+8), roughly corresponding to the period when ClNO<sub>2</sub> is  
12 not destroyed by photolysis. Nights with significant amount of missing data for the measurements were excluded.  
13 Figure S2 shows scatter plots of these averages of ClNO<sub>2</sub> against the averages of the other species including their  
14 linear fits. The R<sup>2</sup> for these fits were 0.48, 0.04, and 0.21 for CO<sub>t</sub>, CO<sub>bb</sub> FINN, and CO<sub>bb</sub> GFAS respectively.  
15 The fact that mixing ratios of CO<sub>bb</sub> is so much smaller than CO<sub>t</sub> according to the model, combined with the much  
16 better correlation for CO<sub>t</sub> than for CO<sub>bb</sub> strongly suggests that industrial emissions are the dominant source of  
17 chlorine, rather than biomass burning. To further investigate the source of chloride, the model was also run to  
18 calculate sea salt levels instead of CO. This resulted in a poor correlation between sea salt and the ClNO<sub>2</sub> (figure  
19 S4). The absolute levels of sea salt calculated by the model were also very low, unlikely to be able to produce the  
20 observed mixing ratios of ClNO<sub>2</sub> as observed by CIMS.

21

### 22 **3.4 Particle phase ClNO<sub>2</sub>**

23 A particle desorption profile was observed in the high resolution data for ClNO<sub>2</sub>. The count increase at this 1 AMU  
24 mass can be attributed to two sources; SO<sub>3</sub> and ClNO<sub>2</sub> as shown in Figure 5. The SO<sub>3</sub> peak is predominantly found  
25 in the particle phase and is below limit of detection (LOD) in the gas phase. During initial analysis of the data,  
26 SO<sub>3</sub> interfered with the ClNO<sub>2</sub> peak fitting and attributed its counts to ClNO<sub>2</sub> in the particle phase as its <sup>33</sup>S ion is  
27 only 0.005 AMU away from the ClNO<sub>2</sub> peak. Upon its inclusion into the peak list and utilisation of the Tofware  
28 feature which constrains isotopes and reallocates the signal appropriately, ClNO<sub>2</sub> remains to indicate a strong  
29 desorption profile. The diurnal cycle of these desorptions correlate well with the ClNO<sub>2</sub> gas phase profile,  
30 indicating a correct assignment of the counts to particle phase ClNO<sub>2</sub>. The desorption profiles with respect to  
31 temperature also exhibit a thermogram structure and not e.g. a gas phase leak into the system which could have  
32 accounted for the correlation with the gas phase time series. This suggests the possible presence of ClNO<sub>2</sub> in the  
33 particle phase. Another possible explanation could be the deposition of ClNO<sub>2</sub> from the gas phase onto the filter  
34 as the ambient air flows through the FIGAERO.

35 If we assume the analysis and collection technique is correct, we see an average particle to gas phase partitioning  
36 of 0.07, with a maximum of 0.33 and a minimum of 0.009. The average mixing ratio of ClNO<sub>2</sub> collected onto the  
37 filter during desorption is 13 ppt with a maximum of 120 ppt. Previous modelling studies assume all ClNO<sub>2</sub> is in  
38 the gas phase due to the low Henry's law constant e.g. for the TexAQS II campaign they calculated that 0.1 ppb

1 in the gas phase would yield 0.54 ppt in the particle phase (Simon *et al.*, 2008). However, this data indicates a non-  
2 negligible amount of the chlorine associated with ClNO<sub>2</sub> is not liberated from the particle phase, assuming that no  
3 additional ClNO<sub>2</sub> is formed by thermally driven reactions. The slope of the particle to gas phase CIMS data is  
4 calculated to be 0.048, a factor of 96 higher than using the Henry's law coefficient to estimate the particle mixing  
5 ratio.

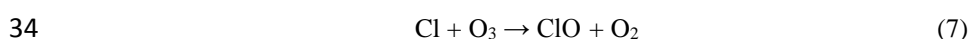
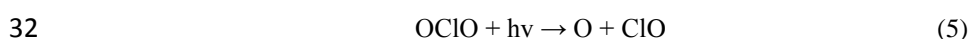
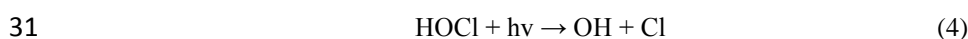
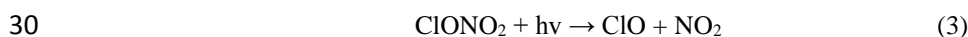
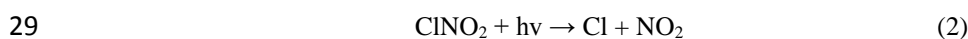
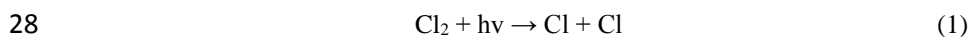
6

### 7 **3.5 ClNO<sub>2</sub> daytime persistence and Cl liberation**

8 Both ClNO<sub>2</sub> and N<sub>2</sub>O<sub>5</sub> are photolytically unstable, with studies reporting lifetimes on the order of hours for ClNO<sub>2</sub>  
9 depending on the solar strength (e.g. Ganske *et al.*, 1992, Ghosh *et al.*, 2011). Nocturnal ClNO<sub>2</sub> removal pathways  
10 have generally been reported to be negligible, with ClNO<sub>2</sub> being assumed to be relatively inert (Wilkins *et al.*,  
11 1974; Frenzel *et al.*, 1998; Rossi, 2003; Osthoff *et al.*, 2008), but the work of Roberts *et al.*, (2008) and Kim *et al.*,  
12 (2014) would suggest that this may not be strictly true. However, given that the average diurnal profile does not  
13 show the importance of nocturnal removal pathways in this study, observed losses are attributed solely to  
14 photolysis, with J(ClNO<sub>2</sub>) controlling the lifetime.

15 Rapid photolysis can be observed for N<sub>2</sub>O<sub>5</sub> in Figure 6 showing a near instant drop below LOD, whereas the ClNO<sub>2</sub>  
16 mixing ratio not only persists for up to 7 hours, but also shows evidence of an increase in mixing ratio at 7 am  
17 (Figure 6). This is observed throughout the campaign and has been frequently observed in the previous study at  
18 Wangdu (Tham *et al.*, 2016). The breakdown of the nocturnal boundary layer and inflow of air masses from above,  
19 carrying pollution from nearby industry/ies is a likely cause of this persistence of possible increase of ClNO<sub>2</sub>. Liu  
20 *et al.* (2017) also observed high daytime mixing ratios of ClNO<sub>2</sub> (60 ppt) at the Wangdu site which they attribute  
21 to a possible oxidation mechanism due its correlation with O<sub>3</sub> and Cl<sub>2</sub> providing a daytime formation pathway to  
22 maintain mixing ratios against its rapid photolysis.

23 Consistent with past measurements and the measurements of this study, ClNO<sub>2</sub> is expected to provide a significant  
24 source of Cl during day time hours, presenting a potentially significant source of the reactive Cl atom during the  
25 day. Its rapid photolysis rate and elevated mixing ratios enables Cl to compete with OH oxidation chemistry, the  
26 known dominant daytime radical source. Here, a simple steady state calculation will be used to determine the Cl  
27 atom mixing ratio summarised below, but detailed within the supplementary:



1

$$2 \quad [\text{Cl}]_{\text{SS}} = \{2J_1[\text{Cl}_2] + J_2[\text{ClNO}_2] + J_3[\text{ClONO}_2] + J_4[\text{HOCl}] + J_5[\text{OCIO}] + k_7 [\text{OH}][\text{HCl}]\} / \{k_7[\text{O}_3] + k_8[\text{CH}_4]_{\text{equivalent}}\}$$

3 (9)

4 Where  $[\text{CH}_4]_{\text{equivalent}}$  represents the reactive VOC present as if it were reacting as  $\text{CH}_4$

5 Bannan et al., (2105), were able to use this steady state approach to compare the relative loss via reaction with OH  
6 compared with Cl atoms. Although this approach is an estimation, it was shown to produce comparable to results  
7 with that of the more rigorous MCM approach. Steady state calculations reveal a sharp rise of chlorine atoms  
8 produced at sunrise peaking at  $1.6 \times 10^5$  molecules  $\text{cm}^3$  around 7 am which then gradually decreases, contributing  
9 to Cl atom production until 2 pm (Figure 7a). Supporting  $\text{Cl}_2$ ,  $\text{ClONO}_2$ ,  $\text{OCIO}$ ,  $\text{HOCl}$  and  $\text{HCl}$  measurements by  
10 CIMS report that chlorine atoms can sustain a relatively high production rate until 3 pm as evidenced by the  
11 daytime build-up of  $\text{HCl}$  and  $\text{Cl}_2$ .  $\text{ClNO}_2$  on average contributes to 78% of the chlorine atoms produced from  
12 inorganic halogens with 13% from  $\text{Cl}_2$ .  $\text{ClNO}_2$  also represents over 50% of the chlorine atoms until midday. After  
13 ca. 3 pm  $\text{Cl}_2$  and  $\text{HCl}$  becomes the more dominant Cl atom source. On the night where the highest  $\text{ClNO}_2$  mixing  
14 ratios were measured, 90% of the chlorine atoms originated from  $\text{ClNO}_2$  photolysis until 2 pm and  $\text{HCl}$  and  $\text{Cl}_2$   
15 then become main contributors sustaining until 4 pm (up to 80%).  $\text{ClONO}_2$ ,  $\text{HOCl}$  and  $\text{OCIO}$  appear to be  
16 insignificant contributors to chlorine atom throughout the campaign compared with  $\text{ClNO}_2$ ,  $\text{HCl}$  and  $\text{Cl}_2$ .

17 To put these chlorine atom mixing ratios into a more global perspective, data collected by the University of  
18 Manchester from a marine site and an urban European site have been compared in Figure 7b. Bannan et al., (2015)  
19 and (2017) previously utilised a box model to calculate Cl atom mixing ratios during the campaign so that the rate  
20 of oxidation of VOCs by Cl atoms could be compared with oxidation by measured OH and measured ozone. The  
21 simple steady state calculation described previously will be used to determine the Cl atom mixing ratio for both  
22 this measurement study. The results show that both at the UK marine and urban site max chlorine atom mixing  
23 ratios are more than an order of magnitude lower than the mean of Beijing. It should however be noted that the  
24 only source of Cl in the UK studies was  $\text{ClNO}_2$ , but given the dominance of  $\text{ClNO}_2$  in this study the measurements  
25 presented here suggest a high importance of the chlorine chemistry for the Asian air chemistry. Studies of chloride  
26 radical production in Los Angeles by Riedel *et al.* (2012) and Young *et al.* (2014) indicate that the high production  
27 rate in Beijing is somewhat typical of urban sites, although  $\text{HCl}$  and  $\text{ClNO}_2$  contribution to radical production is  
28 the same, whereas here we see very little chloride radical production from  $\text{HCl}$  in comparison to  $\text{ClNO}_2$ .

29 Although this study does not reach the scope of characterising  $\text{O}_3$  and  $\text{RO}_x$  production from chlorine atom  
30 chemistry, statistics are often reported with  $\text{ClNO}_2$  morning chemistry via modelling simulations, we can put into  
31 perspective the mean and maximum mixing ratios relative to other studies. Tham *et al.* (2016) recorded a maximum  
32  $\text{ClNO}_2$  mixing ratio of 2070 ppt from a plume originating from Tianjin, the closest megacity to Beijing, and report  
33 a 30% increase in  $\text{RO}_x$  production and up to 13% of  $\text{O}_3$  production. Liu *et al.* (2017) observed peak mixing ratios  
34 up to 3 ppb and similar diurnal mixing ratios which they calculated contributes to a 15% enhancement of peroxy  
35 radicals and 19%  $\text{O}_3$  production. Wang *et al.* (2016) report up to 4.7 ppb of  $\text{ClNO}_2$  in Hong Kong and calculated  
36 a maximum increase of 106% of  $\text{HO}_x$  in the morning and an enhancement of following daytime  $\text{O}_3$  production up  
37 to 41%. It is therefore evident that this work supports similar studies in Asia that conclude that chlorine atom  
38 oxidation significantly contributes to atmospheric oxidation via  $\text{RO}_x$  and  $\text{O}_3$  production. Although several studies

1 have demonstrated a non-negligible impact of chlorine oxidation chemistry (e.g. Oshoff et al., 2008, Riedel et al.,  
2 2014 and Sarwar et al., 2014), the impact of Cl chemistry varies significantly between various areas and  
3 atmospheric conditions, e.g. Bannan et al., 2015, 2017 deemed the impact from chlorine atom chemistry to be  
4 relatively low with respect to O<sub>3</sub> production and competing with OH radicals for VOC oxidation”

5

### 6 **3.6 VOC oxidation by chlorine atoms**

7 Steady state calculations of OH (as described by Whalley *et al.*, 2010) estimate that campaign average maximum  
8 mixing ratio was  $7 \times 10^6$  molecules cm<sup>3</sup> (Figure 7b), 6 times greater than the maximum chlorine atom mixing ratio  
9 and 14 times higher than the average chlorine atom mixing ratio. Pszeny *et al.* (2007) report estimated OH to  
10 chlorine atom ratios, from VOC lifetime variability relationships, of 45 to 199 along the East Coast of the United  
11 States. Although the ratio appears much larger than calculated in this work, here we present not only significantly  
12 high mixing ratios of ClNO<sub>2</sub> which are appearing to be a consistent conclusion from measurements in Asia, but  
13 also the chlorine within this study appears to originate from an anthropogenic origin rather than marine, possessing  
14 the ability to supply a much larger reservoir of halogens to be liberated through photolysis.

15 The relative oxidation rate of the chlorine atom and OH to VOCs can vary greatly. Rate coefficients for reaction  
16 of Cl atoms with some volatile organic compounds have been shown to be up to 200 times faster than the  
17 comparable reaction with OH. The ratio reported here is significantly less than this each day, Cl can subsequently  
18 dominate VOC oxidation for some fraction of the day. Here, the diurnal maxima of the chlorine atom and OH  
19 differs by 5 hours, enabling chlorine atoms to clearly dominate VOC oxidation earlier in the day before OH mixing  
20 ratios have built up. The relative oxidation rate of VOCs to OH and the chlorine atom also varies greatly, creating  
21 a difference for various VOCs. If an average reaction rate for alkenes and alkanes to Cl and OH is calculated, it is  
22 possible to generalise the significance of each oxidation pathway to qualitatively assess the contribution chlorine  
23 atoms have on oxidation chemistry. It can be seen in Figure 8 that alkenes are much more likely to be oxidised by  
24 OH than Cl, although a significant contribution (15%) is attributed to chlorine chemistry. Although significant if  
25 evaluated on a global level, Liu *et al.*, (2017) estimated that Cl atoms oxidize slightly more alkanes than OH  
26 radicals in a similar region of China, implying the increased scale of chlorine oxidation in China. Alkanes are  
27 known to have a much higher Cl to OH relative reaction rate than alkenes and Cl contribution to oxidation is higher  
28 than OH until midday. The contribution to oxidation remains almost equal for the remainder of the day due to the  
29 persistence of ClNO<sub>2</sub> and also relatively high levels of Cl<sub>2</sub> and HCl. This analysis is representative of that by  
30 Bannan *et al.* (2015) who report contributions of alkene and alkane oxidation by Cl up to 3 and 15% respectively  
31 from ClNO<sub>2</sub> mixing ratios peaking at 724 ppt.

32 This significant oxidation of VOCs by chlorine atoms will result in different products to that of OH oxidation as  
33 illustrated that neglecting the contributions made by Cl atoms will significantly underestimate the degree of  
34 chemical processing of VOCs in this study, and other environments where there is a source of Cl atoms. Evidence  
35 of the proposed Cl oxidation of VOCs is validated through detection of selected Cl induced oxidation products by  
36 the ToF-CIMS, all of which are displayed in Table 1.

37

### 1 3.6.1 Isoprene oxidation by the chlorine atom

2 1-Chloro-3-methyl-3-butene-2-one (CMBO,  $C_5H_6ClO$ ), a unique marker of chlorine chemistry, has previously  
3 been measured at mixing ratios up to 9 ppt by offline gas chromatography in Houston Texas (Tanaka *et al.*, 2003)  
4 and in laboratory studies of chlorine-isoprene oxidation (Wang *et al.* (2017)). CMBO exhibited a campaign  
5 maximum of 13.2 ppt and mean of 5.16 ppt exhibiting a near typical diurnal profile with mixing ratios rising  
6 sharply after sunrise, at the same rate as the chlorine atom production but maintaining mixing ratios past noon  
7 longer than that of isoprene and the chlorine atom.

8 The daily maxima of CMBO varied throughout the campaign and can be explained by the relative mixing ratios  
9 of its precursors; the chlorine atom and isoprene. Its mixing ratio throughout the campaign followed similar  
10 intensities to its precursors and figure 9 highlights its dependence on both Cl atom and isoprene mixing ratios. The  
11 production rate of Cl and mixing ratio of isoprene were relatively low from the 24<sup>th</sup> to the 27<sup>th</sup> of May ( $1.6 \times 10^5$   
12 molecules  $cm^{-3} s^{-1}$  Cl and 0.5 ppb isoprene), which resulted in relatively low CMBO mixing ratios. An increase in  
13 isoprene and Cl on the 28<sup>th</sup> to the 30<sup>th</sup> May was subsequently mirrored by the CMBO levels as qualitatively  
14 expected. On closer inspection of the 30<sup>th</sup> and 31<sup>st</sup> May, the mixing ratio of CMBO was lower than expected on  
15 the 30<sup>th</sup> due to higher chlorine atom and isoprene mixing ratios compared to the 31<sup>th</sup>. This could be explained by  
16 anticipated higher OH mixing ratio as calculated by the steady state model, which is also further represented by  
17 higher mixing ratios of IEPOX (isoprene epoxydiols, i.e. OH oxidation products) on the 30<sup>th</sup>. This illustrates how  
18 the ToF-CIMS can identify isoprene oxidation products of two competing oxidation pathways. The high levels of  
19 IEPOX on the 28<sup>th</sup> May can also possibly describe the relatively high levels of CMBO in the particle phase due to  
20 an already well oxidised air mass. CMBO may also not be unique to only isoprene-chloride reactions and therefore  
21 have alternative sources not represented in this data set.

22 Further daily oxidation rates can be probed via analysis of the related isoprene oxidation products observed by the  
23 CIMS. Figure 10 depicts the diurnal time series of the precursor itself and several Cl-VOC products and IEPOX.  
24 CMBO mixing ratios rise rapidly after sunrise due to the low mixing ratio of OH and high production rate of the  
25 chlorine atom. The secondary and tertiary products,  $C_5H_9ClO_2$  and  $C_5H_9ClO_3$  (also measured in the laboratory by  
26 Wang *et al.*, 2017) increased in mixing ratio at a much slower rate, but appear to peak later in the day (4 pm)  
27 whereas CMBO peaked around 10 am (similar to the  $ClNO_2$  peak time) and fall off, due to its further oxidation to  
28 form the secondary and tertiary products. IEPOX mixing ratios increased slowly after sunrise and peaked later in  
29 the day, as expected due to the availability of OH and competition from the chlorine atom chemistry. The similar  
30 time series of the secondary and tertiary products to IEPOX was also reported by Wang *et al.*, (2017) and were  
31 suggested to be ideal tracers of SOA production.

32

### 33 3.6.2 Anthropogenic Cl-VOC production

34 A similar unique chlorine oxidation marker in urban coastal areas, has been reported in the literature for 1, 3  
35 butadiene; 4-chlorocrotonaldehyde (CCA) (Wang *et al.*, 2000). No measurements of 1, 3 butadiene were made  
36 during this field campaign, although due to its common source to benzene (automobile exhausts (Ye *et al.*, 1998),  
37 we present a comparison of the CCA measured by CIMS and benzene measurements made by the PTR-MS. The

1 intensity of CCA in both the gas and particle phase with mixing ratio in the gas phase up to 13 ppt reflect well the  
2 mixing ratios of its precursors. The maximum mixing ratio of the chlorine atom coincides with a high mixing ratio  
3 of benzene and subsequently CCA on the 30<sup>th</sup> May whereas very low levels of CCA were observed for the  
4 beginning of the campaign (Figure 11).

5 The diurnal time series of benzene (Figure 12) indicates high mixing ratios in the early hours of the day, possibly  
6 associated with high anthropogenic activity or an inflow of urban air masses from downtown Beijing. The mixing  
7 ratio falls off throughout the day and almost perfectly anti correlates with the CCA gas phase diurnal profile which  
8 increases from sunrise and peaks at 3 pm. The particle phase CCA diurnal time series steadily builds up throughout  
9 the day and do not peak until late in the evening, providing evidence of SOA production from the chlorine oxidation  
10 of anthropogenic pollutants.

11

#### 12 **4. Conclusions**

13 A FIGAERO ToF-CIMS was utilised in Beijing to assess the liberation of chlorine atoms via inorganic halogen  
14 photolysis. A suite of inorganic halogens were detected, namely ClNO<sub>2</sub> reaching mixing ratios up to 2900 ppt,  
15 which is suggested to have an anthropogenic origin due to the particulate chlorine correlation with SO<sub>2</sub>, benzene  
16 and CO. ClNO<sub>2</sub> was identified in the particle phase at higher ratios with respect to its gas phase component than  
17 expected, which may only prove to be significant at such elevated mixing ratios as observed in East Asia. ClNO<sub>2</sub>  
18 mixing ratios above LOD persisted up to 7 hours past sunrise, attributed to the lifetime of ClNO<sub>2</sub> at these high  
19 mixing ratios and a possible in-flow of heavily polluted air masses from the downtown urban area. Supporting Cl<sub>2</sub>  
20 and HCl mixing ratios proved to be significant contributors to chlorine atom production via steady state  
21 calculations enabling an average daytime peak mixing ratio of chlorine atoms of  $1.6 \times 10^5$  molecules cm<sup>-3</sup>.  
22 Compared with data attained from European based campaigns, these mixing ratios exceed marine and urban  
23 environments by at least an order of magnitude.

24 This high mixing ratio of chlorine atoms resulted in a steady state calculated OH:Cl ratios down to a factor of 6,  
25 enabling Cl chemistry to not only dominate alkane oxidation until midday but contribute significantly to alkene  
26 oxidation throughout the day (15% on average). This enabled significant mixing ratios of Cl-VOCs to be formed  
27 providing the first ambient high time resolution measurements of specific Cl-VOC species simultaneously  
28 measured in the gas and particle phase. The measured unique markers of chlorine chemistry for both biogenic and  
29 anthropogenic precursors provides quantitative and qualitative data to probe the extent of chlorine atom chemistry  
30 and how they compete with OH. Simultaneous measurements of the VOC precursors via PTR-MS, and IEPOX,  
31 Cl-VOCs with the CIMS provides rich information on SOA formation pathways via both OH and chlorine atom  
32 oxidation. Multistep oxidation products of Cl-VOCs were also identified and can provide partitioning information  
33 and SOA formation rates and lifetimes.

34 The results highlight deficiency in chlorine atom chemistry descriptions within models possibly due to a lack in  
35 quantification and identification of Cl-VOC products in gas and particle phase. This work provides instrumental  
36 capability to probe the competition between OH and Cl oxidation chemistry and quantify their effect on ozone and  
37 SOA formation.

1 **Acknowledgement:**

2 The work was done under the framework research program on ‘Photochemical smog in China’ financed by  
3 Swedish Research Council (639-2013-6917). The National Natural Science Foundation of China (21677002) and  
4 the National Key Research and Development Program of China (2016YFC0202003) also helped fund this work.  
5

6 **References**

- 7 Allan, W., Struthers, H. and Lowe, D. C.: Methane carbon isotope effects caused by atomic chlorine in the marine  
8 boundary layer: Global model results compared with southern hemisphere measurements. *J. Geophys. Res.* 112,  
9 2007.
- 10 AQIRP, 1995, Effects of gasoline T50, T90 and sulfur on exhaust emissions of current and future technology  
11 vehicles. Auto/Oil Air Quality Improvement Research Program, Technical Bulletin No. 18.
- 12 Baker, A. K., Sauvage, C., Thorenz, U. R., van Velthoven, P., Oram, D. E., Zahn, A., Berninkmeijer, C. A. M.  
13 and Williams, J.: Evidence for strong, widespread chlorine atom chemistry associated with pollution outflow  
14 from continental Asia, *Sci. Rep.*, 6, 36821, 2016.
- 15 Bannan, T. J., Booth, A. M., Bacak, A., Muller, J. B. A., Leather, K. E., Le Breton, M., Jones, B., Young, D., Coe,  
16 H., Allan, J., Visser, S., Slowik, J. G., Furger, M., Prevot, A. S. H., Lee, J., Dunmore, R. E., Hopkins, J. R.,  
17 Hamilton, J. F., Lewis, A. C., Whalley, L. K., Sharp, T., Stone, D., Heard, D. E., Fleming, Z. L., Leigh, R.,  
18 Shallcross, D. E., and Percival, C. J.: The first UK measurements of nitryl chlorine using a chemical ionization  
19 mass spectrometer in central London in the summer of 2012, and an investigation of the role of Cl atom oxidation,  
20 *J. Geophys. Res. Atmos.*, 120, 5638–5657, 2015.
- 21 Bannan, T. J., Bacak, A., Le Breton, M., Ouyang, B., Flynn, M., McLeod, M., Jones, R., Malkin, T. L., Whalley,  
22 L. K., Heard, D. E., Bandy, B., Khan, A., Shallcross, D. E., and Percival, C. J.: Ground and airborne U.K.  
23 measurements of nitryl chloride, an investigation of the role of Cl atom oxidation at Weybourne Atmospheric  
24 Observatory, *J. Geophys. Res. Atmospheres*, 10.2017.
- 25 Brown, S. S. & Stutz, J. Nighttime radical observations and chemistry *Chem. Soc. Rev.*, The Royal Society of  
26 Chemistry, 41, 6405-6447, 2012.
- 27 Burkholder, J.B. et al. *Chemical Kinetics and Photochemical Data for Use in Atmospheric Studies: Evaluation*  
28 *Number 18.* Jet Propulsion Laboratory, California Institute of Technology, Pasadena, CA, 2015.
- 29 Cai, X., Ziemba, L. D. and Griffin, R. J.: Secondary aerosol formation from the oxidation of toluene by chlorine  
30 atoms, *Atmos. Environ.*, 42, 32, 2008.
- 31 Brown, S. S., Stark, H., and Ravishankara, A. R.: Applicability of the steady state approximation to the  
32 interpretation of atmospheric observations of NO<sub>3</sub> and N<sub>2</sub>O<sub>5</sub>, *J. Geophys. Res.- Atmos.*, 108, 4539, 2003.
- 33 Brown, S. S., Dube, W. P., Tham, Y. J., Zha, Q. Z., Xue, L. K., Poon, S., Wang, Z., Blake, D. R., Tsui, W., Parrish,  
34 D. D., Wang, T.: Nighttime chemistry at a high altitude site above Hong Kong, *J. Geophys. Res. Atmos.*, Vol. 121,  
35 Issue. 5, 2457-2475, 2016.  
36
- 37 DeCarlo, P. F., Kimmel, J., Trimborn, A., Northway, M., Jayne, J. T., Aiken, A., Gonin, M., Fuhrer, K., Horvath,  
38 T., Docherty, K., Worsnop, D. R., and Jimenez, J. L.: Field-deployable, high-resolution, time-of-flight Aerosol  
39 Mass Spectrometer, *Anal. Chem.*, 78, 8281–8289, 2006.
- 40 de Gouw, J. and Warneke, C.: Measurements of volatile organic compounds in the earth’s atmosphere using  
41 proton-transferreaction mass spectrometry, *Mass Spectrom. Rev.*, 26, 223–257, 2007.



- 1 Faxon, C. B., Bean, J. K., and Ruiz, L. H.: Inland Mixing ratios of Cl<sub>2</sub> and ClNO<sub>2</sub> in Southeast Texas suggest  
2 chlorine chemistry significantly contributes to atmospheric reactivity, *Atmosphere*, 6, 1487–1506, 2015.
- 3 Finley, B. D. and Saltzman, E. S.: Measurement of Cl<sub>2</sub> in coastal urban air, *Geophys. Res. Lett.*, 33, 2006.
- 4 Fraser, M. P., G. R. Cass, B. R. Simoneit, & R. A. Rasmussen (1997). Air quality model evaluation data for  
5 organics. 4. C<sub>2</sub>-C<sub>36</sub> non-aromatic hydrocarbons. *Environmental science & technology*, 31(8), 2356-2367  
6 DOI: 10.1021/es960980g
- 7 Hoffman, R. C., Gebel, M. E., Fox, B. S., and Finlayson-Pitts, B. J.: Knudsen cell studies of the reactions of  
8 N<sub>2</sub>O<sub>5</sub> and ClONO<sub>2</sub> with NaCl: Development and application of a model for estimating available surface areas  
9 and corrected uptake coefficients, *Phys. Chem. Chem. Phys.*, 5, 9, 1780–1789, 2003.
- 10 Hofzumahaus, Andreas, Franz Rohrer, Keding Lu, Birger Bohn, Theo Brauers, Chih-Chung Chang, Hendrik  
11 Fuchs, et al. "Amplified Trace Gas Removal in the Troposphere." *Science* 324, no. 5935 (2009): 1702.
- 12 Hu, W. W., Hu, M., Yuan, B., Jimenez, J. L., Tang, Q., Peng, J. F., Hu, W., Shao, M., Wang, M., Zeng, L. 74 M.,  
13 Wu, Y. S., Gong, Z. H., Huang, X. F., and He, L. Y.: Insights on organic aerosol aging and the influence of  
14 coal combustion at a regional receptor site of central eastern China, *Atmos. Chem. Phys.*, 13, 10095-10112,  
15 2013.
- 16 Hu, W., Hu, M., Hu, W., Jimenez, J. L., Yuan, B., Chen, W., Wang M., We, Y., Chen, C., Wang, Z., Peng, J.,  
17 Zeng, L. and Shao, M. Chemical composition, sources, and aging process of submicron aerosols in Beijing:  
18 Contrast between summer and winter, *J. Geophys. Res.*, 121, 4, 1955-1977, 2016.
- 19 Huang, M., Liu, X., Hu, C., Guo, X., Gu, X., Zhao, W., Wang, Z., Fang, L. and Zhang, W.: Aerosol laser time-of-  
20 flight mass spectrometer for the on-line measurement of secondary organic aerosol in smog chamber, *Meas. J. Int.*  
21 *Meas. Confed.*, 55(3), 394–401, 2014.
- 22 Keil, A. and Shepson, P.: Chlorine and bromine atom ratios in the springtime Arctic troposphere as determined  
23 from measurements of halogenated volatile organic compounds, *J. Geophys. Res.*, 111, 2006.
- 24 Kaiser, J. W., Heil, A., Andreae, M. O., Benedetti, A., Chubarova, N., Jones, L., Morcrette, J.-J., Razinger, M.,  
25 Schultz, M. G., Suttie, M., and van der Werf, G. R. (2012). Biomass burning emissions estimated with a global  
26 fire assimilation system based on observed fire radiative power. *Biogeosciences*, 9:527-554.
- 27 Kercher, J. P., Riedel, T. P., and Thornton, J. A.: Chlorine activation by N<sub>2</sub>O<sub>5</sub>: simultaneous, in situ detection of  
28 ClNO<sub>2</sub> and N<sub>2</sub>O<sub>5</sub> by chemical ionization mass spectrometry, *Atmos. Meas. Tech.*, 2, 193–204, doi:10.5194/amt-  
29 2-193-2009, 2009.
- 30 Khan, M. A. H., Ashfold, M. J., Nickless, G., Martin, D., Watson, L. A., Hamer, P. D., Wayne, R. P., Canosa-  
31 Mas, C. E. and Shallcross, D. E.: Night-time NO<sub>3</sub> and OH radical mixing ratios in the United Kingdom inferred  
32 from hydrocarbon measurements, *Atmos. Sci. Lett.*, 9, 3, 140-146, 2008.

1 Kim, M. J., Farmer, D. K. and Bertram, T. H.: A controlling role for the air–sea interface in the chemical  
2 processing of reactive nitrogen in the coastal marine boundary layer, *PNAS*, 111 (11), 2943–3948, 2014.  
3

4 Lopez-Hilfiker, F. D., Mohr, C., Ehn, M., Rubach, F., Kleist, E., Wildt, J., Mentel, Th. F., Lutz, A., Hallquist, M.,  
5 Worsnop, D., and Thornton, J. A.: A novel method for online analysis of gas and particle composition: description  
6 and evaluation of a Filter Inlet for Gases and AEROSols (FIGAERO), *Atmos. Meas. Tech.* 2014, 7, 983–1001,  
7 doi:10.5194/amt-7-983-2014.

8 Le Breton, M, Bannan, T. J., Shallcross, D. E., Khan, M. A., Evans, M. J., Lee, J., Lidster, R., Andrews, S.,  
9 Carpenter, L., Schmidt, J., Jacob, D., Harris, N. R. P., Bauguutte, S-J., Gallagher, M., Bacak, A., Leather, K. E.  
10 and Percival, C. J.: Enhanced ozone loss by active inorganic bromine chemistry in the tropical troposphere, *Atmos.*  
11 *Environ.*, 155, 21–28, 2017a.

12 Le Breton, M., Wang, Y., Hallquist, Å. M., Pathak, R. K., Zheng, J., Yang, Y., Shang, D., Glasius, M., Bannan,  
13 T. J., Liu, Q., Chan, C. K., Percival, C. J., Zhu, W., Lou, S., Topping, D., Wang, Y., Yu, J., Lu, K., Guo, S., Hu,  
14 M., and Hallquist, M.: Online gas and particle phase measurements of organosulfates, organosulfonates and  
15 nitrooxyorganosulfates in Beijing utilizing a FIGAERO ToF-CIMS, *Atmos. Chem. Phys. Discuss.*,  
16 <https://doi.org/10.5194/acp-2017-814>, in review, 2017b.

17 Liu, J., D’Ambro, E. L., Lee, B. H., Lopez-Hilfiker, F., Zaveri, R. A., RiveraRios, J. C., Keutsch, F. N., Lyer, S.,  
18 Kurtne, T., Zhang, Z., Gold, A., Surratt, J. D., Shilling, J. E. and Thornton, J. A.: Efficient Isoprene Secondary  
19 Organic Aerosol Formation from a Non-IEPOX Pathway, *Environ. Sci. Technol.*, 50, 18, 9872–9880, 2016.

20 Lopez-Hilfiker, F. D., Mohr, C., Ehn, M., Rubach, F., Kleist, E., Wildt, J., Mentel, Th. F., Lutz, A., Hallquist, M.,  
21 Worsnop, D., and Thornton, J. A.: A novel method for online analysis of gas and particle composition: description  
22 and evaluation of a Filter Inlet for Gases and AEROSols (FIGAERO), *Atmos. Meas. Tech.* 2014, 7, 983–1001,  
23 doi:10.5194/amt-7-983-2014.

24 Ma, Q., Shuxiao, S. C., Zhao, B., Martin, R. V., Brauer, M., Cohen, A., Jiang, J., Zhou, W., Hao, J., Frostad, J.,  
25 Forouzanfar, M. H. and Burnett, T.: Impacts of coal burning on ambient PM1 pollution in China, *Atmos. Chem.*  
26 *Phys.*, 17, 4477–4491, 2017.

27 Manion, J. A., R. E. Huie, R. D. Levin, D. R. Burgess Jr, V. L Orkin, W. Tsang, W. S. McGivern, J. W. Hudgens,  
28 V. D. Knyazev, D. B Atkinson, E. Chai, A. M. Tereza, C.-Y. Lin, T. C. Allison, W. G. Mallard, F. Westley, J.  
29 T. Herron, R. F. Hampson, and D. H. Frizzell (2014) NIST Chemical Kinetics Database, NIST Standard Reference  
30 Database 17, Version 7.0 (Web Version), Release 1.6.8, Data version 2013.03, National Institute of Standards and  
31 Technology, Gaithersburg, Maryland, 20899-8320. Web address: <http://kinetics.nist.gov/>

32 Mielke, L. H., Furgeson, A., Odam-Ankrah, C. A., and Osthoff, H. D.: Ubiquity of ClNO<sub>2</sub> in the urban boundary  
33 layer of Calgary, AB, Canada, *Canadian J. Chem.*, 2015.

34 Nordmeyer, T., Wang, W., Ragains, M. L., Finlayson-Pitts, B. J., Spicer, C. W. and Plastridge, R. A.: Unique  
35 products of the reaction of isoprene with atomic chlorine: Potential markers of chlorine atom chemistry, *Geophys.*  
36 *Res. Lett.*, 24(13), 1615–1618, doi:10.1029/97GL01547, 1997.

37 Ofner, J., Balzer, N., Buxmann, J., Grothe, H., Schmitt-Kopplin, P., Platt, U. and Zetzsch, C.: Halogenation  
38 processes of secondary organic aerosol and implications on halogen release mechanisms, *Atmos. Chem. Phys.*,  
39 12(13), 5787–5806, doi:10.5194/acp-12-5787-2012, 2012.

40 Orlando, J. J., Tyndall, G. S., Apel, E. C., Riemer, D., and Paulson, S. E.: Rate coefficients and mechanisms of the  
41 reaction of Cl-atoms with a series of unsaturated hydrocarbons under atmospheric conditions, *Int. J. Chem. Kinet.*,  
42 35, 334–353, 2003.

43 Osthoff, H.D.; Roberts, J.M.; Ravishankara, a. R.; Williams, E.J.; Lerner, B.M.; Sommariva, R.; Bates, T.S.;  
44 Coffman, D.; Quinn, P.K.; Dibb, J.E.: High levels of nitryl chlorine in the polluted subtropical marine boundary  
45 layer. *Nat. Geosci.* 2008, 1, 324–328, 2008.

- 1 Platt, U., Allan, W., and Lowe, D.: Hemispheric average Cl atom mixing ratio from  $^{13}\text{C}/^{12}\text{C}$  ratios in atmospheric  
2 methane, *Atmos. Chem. Phys.*, 4, 2393–2399, 4, 2004.
- 3 Phillips, G. J., Tang, M. J., Thieser, J., Brickwedde, B., Schuster, G., Bohn, B., Lelieveld, J., and Crowley, J. N.:  
4 Significant mixing ratios of nitryl chlorine observed in rural continental Europe associated with the influence of  
5 sea salt chlorine and anthropogenic emissions, *Geophys. Res. Lett.*, 39, L10811, 2016.
- 6 Phillips, G. J., Thieser, J., Tang, M., Sobanski, N., Schuster, G., Fachinger, J., Drewnick, F., Borrmann, S.,  
7 Bingemer, H., Lelieveld, J. and Crowley, J. N.: Estimating  $\text{N}_2\text{O}_5$  uptake coefficients using ambient measurements  
8 of  $\text{NO}_3$ ,  $\text{N}_2\text{O}_5$ ,  $\text{ClNO}_2$  and particle-phase nitrate, *Atmos. Chem. Phys.*, 16, 13231-13249, 2016.
- 9 Pszenny, A. A. P., Fischer, E. V., Russo, R. S., Sive, B. C., and Varner, R. K.: Estimates of Cl atom mixing ratios  
10 and hydrocarbon kinetic reactivity in surface air at Appledore Island, Maine (USA), during International  
11 Consortium for Atmospheric Research on Transport and Transformation/Chemistry of Halogens at the Isles of  
12 Shoals, *J. Geop*
- 13 Riedel, T. P., Bertram, T. H., Crisp, T. A., Williams, E. J., Lerner, B. M., Vlasenko, A., Li, S. M., Gilman, J., de  
14 Gouw, J., Bon, D. M., Wagner, N. L., Brown, S. S., and Thornton, J. A.: Nitryl chlorine and molecular chlorine in  
15 the coastal marine boundary layer, *Environ. Sci. Technol.*, 46, 10463–10470, 2012.
- 16 Riedel, T. P., Wolfe, G. M., Danas, K. T., Gilman, J. B., Kuster, W. C., Bon, D. M., Vlasenko, A., Li, S. M.,  
17 Williams, E. J., Lerner, B. M., Veres, P. R., Robert, J. M., Holloway, J. S., Lefer, B., Brown, S.S. and Thornton,  
18 J. A.: An MCM modeling study of nitryl chlorine ( $\text{ClNO}_2$ ) impacts on oxidation, ozone production and nitrogen  
19 oxide partitioning in polluted continental outflow, *Atmos. Chem. Phys.*, 14, 3789-3800, 2014.
- 20 Riemer, D. D., Apel, E. C., Orlando, J. J., Tyndall, G. S., Brune, W. H., Williams, E. J., Lonneman, W. A. and  
21 Neece, J. D.: Unique isoprene oxidation products demonstrate chlorine atom chemistry occurs in the Houston,  
22 Texas urban area, *J. Atmos. Chem.*, 61(3), 227–242, 2008.
- 23 Riva, M., Healy, R. M., Flaud, P. M., Perraudin, E., Wenger, J. C. and Villenave, E.: Gas- and Particle-Phase  
24 Products from the Chlorine-Initiated Oxidation of Polycyclic Aromatic Hydrocarbons, *J. Phys. Chem. A*, 119(45),  
25 11170–11181, doi:10.1021/acs.jpca.5b04610, 2015.
- 26 Roberts, J. M., Osthoff, H. D., Brown, S. S., and Ravishankara, A. R.:  $\text{N}_2\text{O}_5$  oxidizes chloride to  $\text{Cl}_2$  in acidic  
27 atmospheric aerosol, *Science*, 321, 1059–1059, doi:10.1126/science.1158777, 2008.
- 28 Sander, R.: Modeling atmospheric chemistry: Interactions between gas-phase species and liquid cloud/aerosol  
29 particles, *Surv. Geophys.*, 20, 1–31, 1999.
- 30 Sarwar, G., Simon, H., Xing, J., and Mathur, R.: Importance of tropospheric  $\text{ClNO}_2$  chemistry across the Northern  
31 Hemisphere, *Geophys. Res. Lett.*, 41, 4050–4058, 2014.
- 32 Simpson, D., Benedictow, A., Berge, H., Bergström, R., Emberson, L. D., Fagerli, H., Flechard, C. R., Hayman,  
33 G. D., Gauss, M., Jonson, J. E., Jenkin, M. E., Nyíri, A., Richter, C., Semeena, V. S., Tsyro, S., Tuovinen, J.-P.,  
34 Valdebenito, Á., and Wind, P.: The EMEP MSC-W chemical transport model – technical description, *Atmos.*  
35 *Chem. Phys.*, 12, 7825-7865, <https://doi.org/10.5194/acp-12-7825-2012>, 2012.
- 36 Simon, H., Y. Kimura, G. McGaughy, D.T. Allen, S.S. Brown, H.D. Osthoff, J.M. Roberts, 422 D. Byun, and D.  
37 Lee.: Modeling the impact of  $\text{ClNO}_2$  on ozone formation in the 423 Houston area, *J. Geophys. Res.*, 114, D00F03,  
38 424 doi:10.1029/2008JD010732, 2009.
- 39 Skamarock, W. C., J. B. Klemp, J. Dudhia, D. O. Gill, D. M. Barker, M. G Duda, X.-Y. Huang, W. Wang, and J.  
40 G. Powers, 2008: A Description of the Advanced Research WRF Version 3. NCAR-Tech, 113,  
41 doi:10.5065/D68S4MVH

- 1 Tanaka, P. L., Riemer, D. D., Chang, S., Yarwood, G., McDonaldBuller, E. C., Apel, E. C., Orlando, J. J., Silva,  
2 P. J., Jimenez, J. L., Canagaratna, M. R., Neece, J. D., Mullins, C. B., and Allen, D. T.: Direct evidence for  
3 chlorine-enhanced urban ozone formation in Houston, Texas, *Atmos. Environ.*, 37, 1393–1400, 2003.
- 4 Tham, Y., Yan, C., Xue, L., Zha, Q., Wang, X., and Wang, T.: Presence of high nitryl chlorine in Asian coastal  
5 environment and its impact on atmospheric photochemistry, *China Sci. Bull.*, 59, 356–359, doi:10.1007/s11434-  
6 013-0063-y, 2014.
- 7 Thornton, J. A., Kercher, J. P., Riedel, T. P., Wagner, N. L., Cozic, J., Holloway, J. S., Dube, W. P., Wolfe, G. M.,  
8 Quinn, P. K., Middlebrook, A. M., Alexander, B., and Brown, S. S.: A large atomic chlorine source inferred from  
9 mid-continental reactive nitrogen chemistry, *Nature*, 464, 271–274, doi:10.1038/nature08905, 2010.
- 10 Wagner, N. L., Riedel, T. P., Young, C. J., Bahreini, R., Brock, C. A., Dube, W. P., Kim, S., Middlebrook, A. M.,  
11 Öztürk, F., Robert, J. M., Russo, R., Sive, B., Swarthout, R., Thornton, J. A., VandenBoer, T. C., Zhou, Y. and  
12 Brown, S. S.: N<sub>2</sub>O<sub>5</sub> uptake coefficients and nocturnal NO<sub>2</sub> removal rates determined from ambient wintertime  
13 measurements, *Atmos. Chem. Phys.*, 13, 9331–9350, 2013.
- 14 Wang, W. and Finlayson-Pits, B. J.: Unique markers of chlorine atom chemistry in coastal urban areas: The  
15 reaction with 1,3-butadiene in air at room temperature, *J. Geophys. Res.*, 106, 5, 4939–4958, 2001.
- 16 Wang, T., Cheung, T., Li, Y., Yu, X. and Blake, D.: Emission characteristics of CO, NO<sub>x</sub>, SO<sub>2</sub> and indications of  
17 biomass burning observed at a rural site in eastern China. *J. Geophys. Res. Atmos.*, 107, 12, 2002.
- 18 Wang, T., Tham, Y.J., Xue, L., Li, Q., Zha, Q., Wang, Z., Poon, S.C.N., Dube, W.P., Blake, D.R., Louie, P.K.K.,  
19 Luk, C.W.Y., Tsui, W., Brown, S.S.: Observations of nitryl chlorine and modeling its source and effect on ozone  
20 in the planetary boundary layer of southern China. *J. Geophys. Res.* 121, 2476e2489, 2016
- 21 Wang, H., Chen, J. and Lu, K.: Development of a portable cavity-enhanced absorption spectrometer for the  
22 measurement of ambient NO<sub>3</sub> and N<sub>2</sub>O<sub>5</sub>: experimental setup, lab characterizations, and field applications in a  
23 polluted urban environment, *Atmos. Chem. Phys.*, 10, 1465–1479, 2017.
- 24 Wang, X., Wang, H., Xue, L., Wang, T., Wang, L., Gu, R., Wang, W., Than, Y. T., Wang, Z., Yang, L., Chen, J.  
25 and Wang, W.: Observations of N<sub>2</sub>O<sub>5</sub> and ClNO<sub>2</sub> at a polluted urban surface site in North China: High N<sub>2</sub>O<sub>5</sub>  
26 uptake coefficients and low ClNO<sub>2</sub> product yields, *Atmos. Environ.*, 156, 125–134, 2017.
- 27 Wang, Z., Wang, W., Tham, Y. J., Hao, Q. L., Wang, L. W., Xinfeng, W., Wang, L. W. and Wang, T.: Fast  
28 heterogeneous N<sub>2</sub>O<sub>5</sub> uptake and ClNO<sub>2</sub> production in power plant plumes observed in the nocturnal residual layer  
29 over the North China Plain, *Atmos. Chem. Phys. Discuss.*, 2017.
- 30 Wang, D. and Ruiz, L. H.: Secondary organic aerosol from chlorine-initiated oxidation of isoprene, *Atmos. Chem.*  
31 *Phys. Discuss.*, 2017–342, 2017.
- 32 Whalley, L. K., Furneaux, K. L., Goddard, A., Lee, J. D., Mahajan, A., Oetjen, H., Read, K. A., Kaaden, N.,  
33 Carpenter, L. J., Lewis, A. C., Plane, J. M. C., Saltzman, E. S., Wiedensohler, A., and Heard, D. E.: The chemistry  
34 of OH and HO<sub>2</sub> radicals in the boundary layer over the tropical Atlantic Ocean, *Atmos. Chem. Phys.*, 10, 1555-  
35 1576, <https://doi.org/10.5194/acp-10-1555-2010>, 2010.
- 36 Wiedinmyer, C., S. K. Akagi, R. J. Yokelson, L. K. Emmons, J. A. Al-Saadi, J. J. Orlando, and A. J. Soja. "The  
37 Fire Inventory from Ncar (Finn): A High Resolution Global Model to Estimate the Emissions from Open Burning."  
38 *Geoscientific Model Development* 4, no. 3 (2011): 625-41.
- 39 Ye, Y., Galbally, I. E., Weeks, I. A., Duffy, B. L., and Nelson, P. F.: Evaporative emissions of 1,3-butadiene from  
40 petrol-fuelled motor vehicles, *Atmos. Environ.*, 32, 2685–2692, 1998.

1 Young, C. J., Washenfelder, R. A., Roberts, J. M., Mielke, L. H., Osthoff, H. D., Tsai, C., Pikelnaya, O., Stutz, J.,  
 2 Veres, P. R., Cochran, A. K., VandenBoer, T. C., Flynn, J., Grossberg, N., Haman, C. L., Lefer, B., Stark, H.,  
 3 Graus, M., de Gouw, J., Gilman, J. B., Kuster, W. C., and Brown, S. S.: Vertically Resolved Measurements of  
 4 Nighttime Radical Reservoirs; in Los Angeles and Their Contribution to the Urban Radical Budget, Environ. Sci.  
 5 Technol., 46, 10965–10973, doi:10.1021/es302206a, 2012.

6

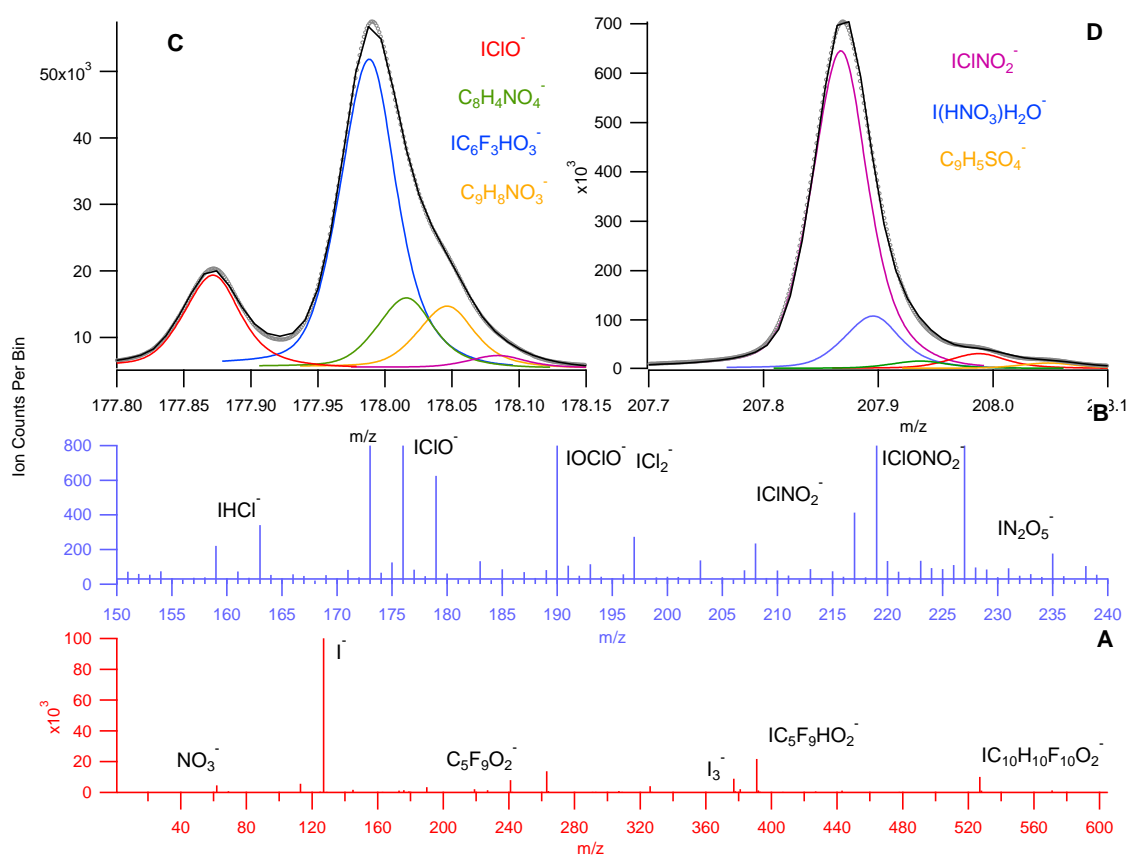
7

8 **Table 1. Identified Cl-VOC reaction products, nomenclature of Cl-VOC and precursor compound.**

Cl-VOC	Potential nomenclature	Precursor
CHClO	formyl chloride	formaldehyde
C <sub>2</sub> H <sub>3</sub> ClO	chloroacetaldehyde	acetaldehyde
C <sub>3</sub> H <sub>5</sub> ClNO <sub>5</sub>	Chloro PPN	PPN
C <sub>2</sub> H <sub>3</sub> ClNO <sub>5</sub>	chloro PAN	PAN
C <sub>3</sub> H <sub>5</sub> ClO	chloroacetone	acetone
C <sub>2</sub> H <sub>3</sub> ClO <sub>2</sub>	chloroacetic acid	acetic acid
CHClO <sub>2</sub>	chloroformic acid	formic acid
C <sub>4</sub> H <sub>7</sub> ClO	chloro MEK or butanal	isoprene
C <sub>5</sub> H <sub>6</sub> ClO	CMBO - chloro 3-methyl-3-butene-2-one	isoprene
C <sub>5</sub> H <sub>9</sub> ClO <sub>2</sub>	-	isoprene
C <sub>5</sub> H <sub>9</sub> ClO <sub>3</sub>	-	isoprene
C <sub>3</sub> H <sub>5</sub> ClO	propanoyl chloride	1, 3 butadiene
C <sub>8</sub> H <sub>9</sub> Cl	chloroethyl benzene	aromatic

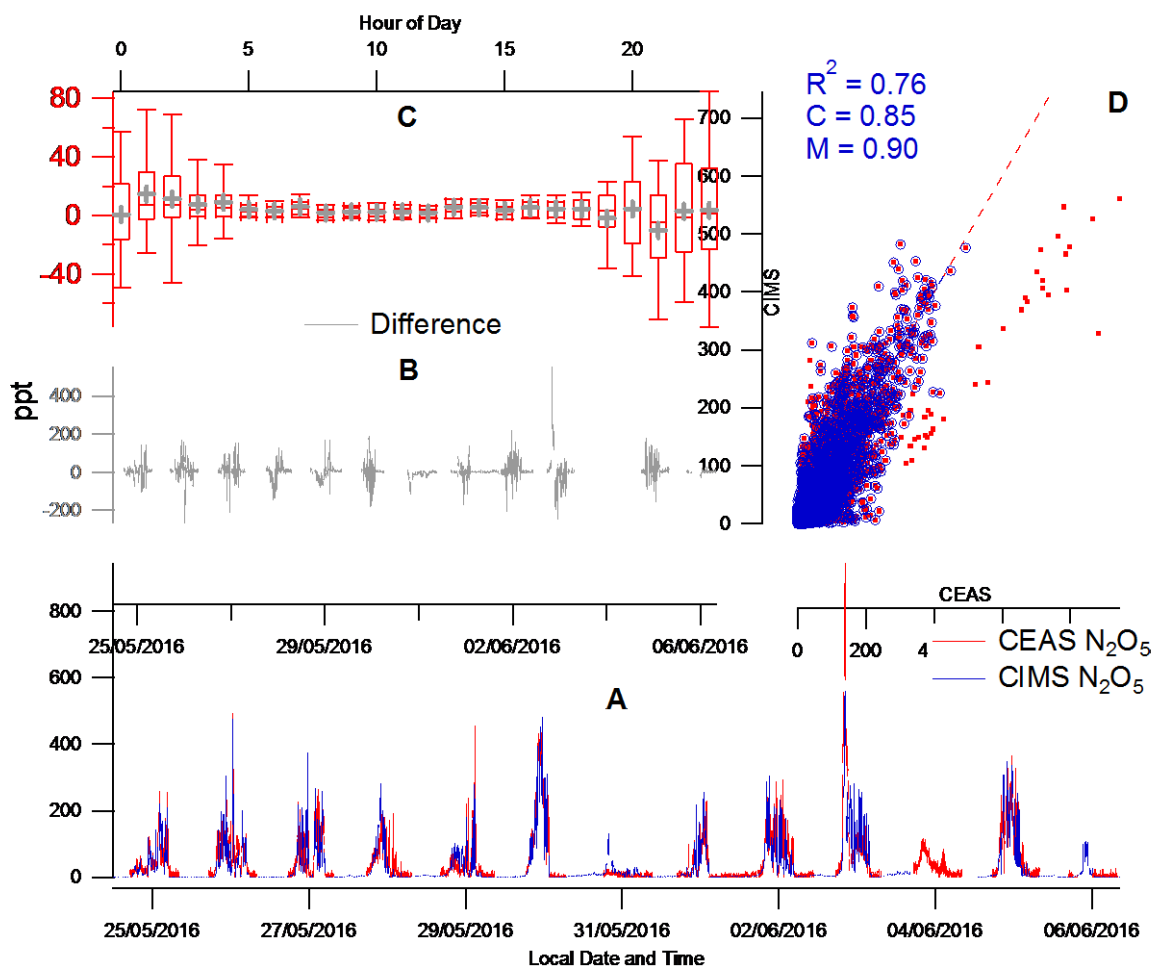
9

10



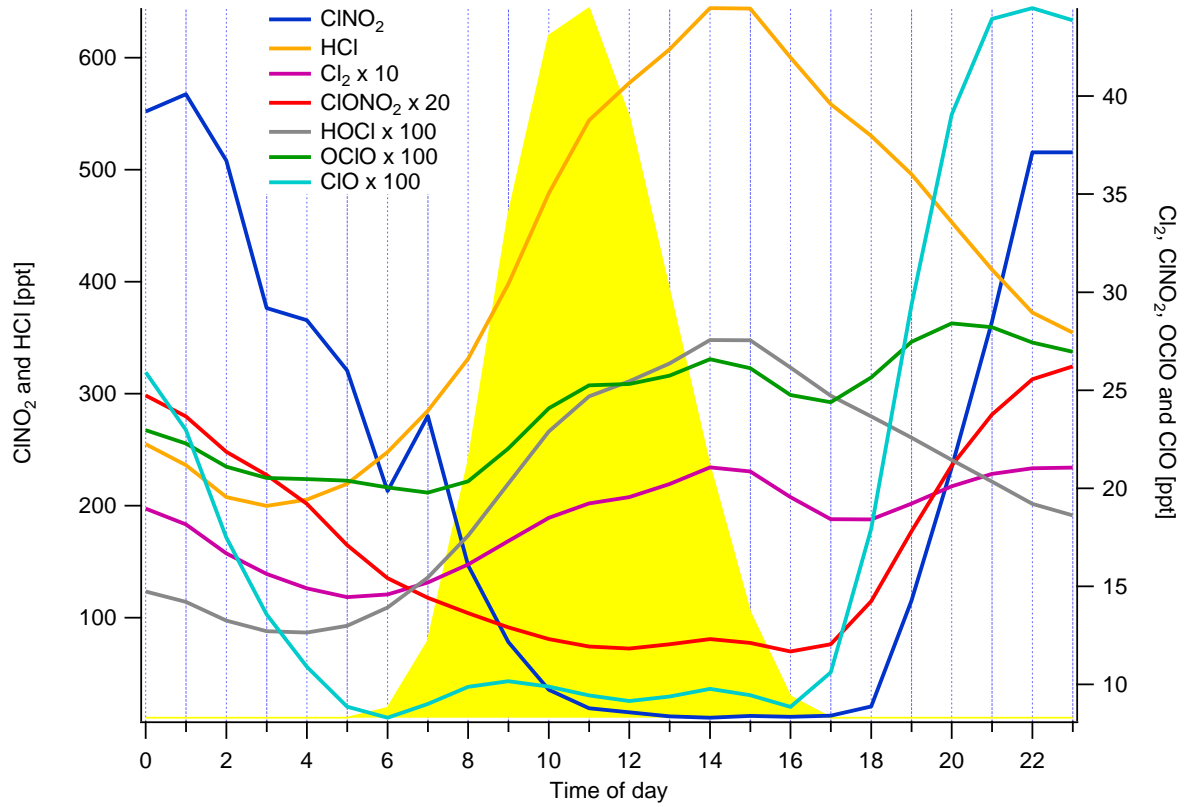
2

3 **Figure 1. Panel A: Average mass spectrum for the whole measured range. Panel B: Average mass spectrum**  
 4 **for the region that contains all gas phase night time species utilised in this work. A high resolution spectral**  
 5 **fit for ClO and ClNO<sub>2</sub> are displayed with corresponding multi peaks with 0.5 AMU (panels C and D). The**  
 6 **black line represents the total fit from all peaks. The grey line represents the mass spectral raw data.**



1  
 2 **Figure 2.** CIMS and CEAS one minute averaged data of  $\text{N}_2\text{O}_5$  with corresponding correlation plot (panel  
 3 **A**), campaign and diurnal deviation (panels **B** and **C** respectively). The red highlighted periods represent  
 4 data collected on the 3<sup>rd</sup> June where a different correlation gradient was observed between CIMS and  
 5 CEAS. The box and whisker plot represents the diurnal difference for the campaign between the CEAS and  
 6 CIMS measurements (panel **D**).  $C$  is the y-intercept of the line of best fit and  $M$  is the gradient.

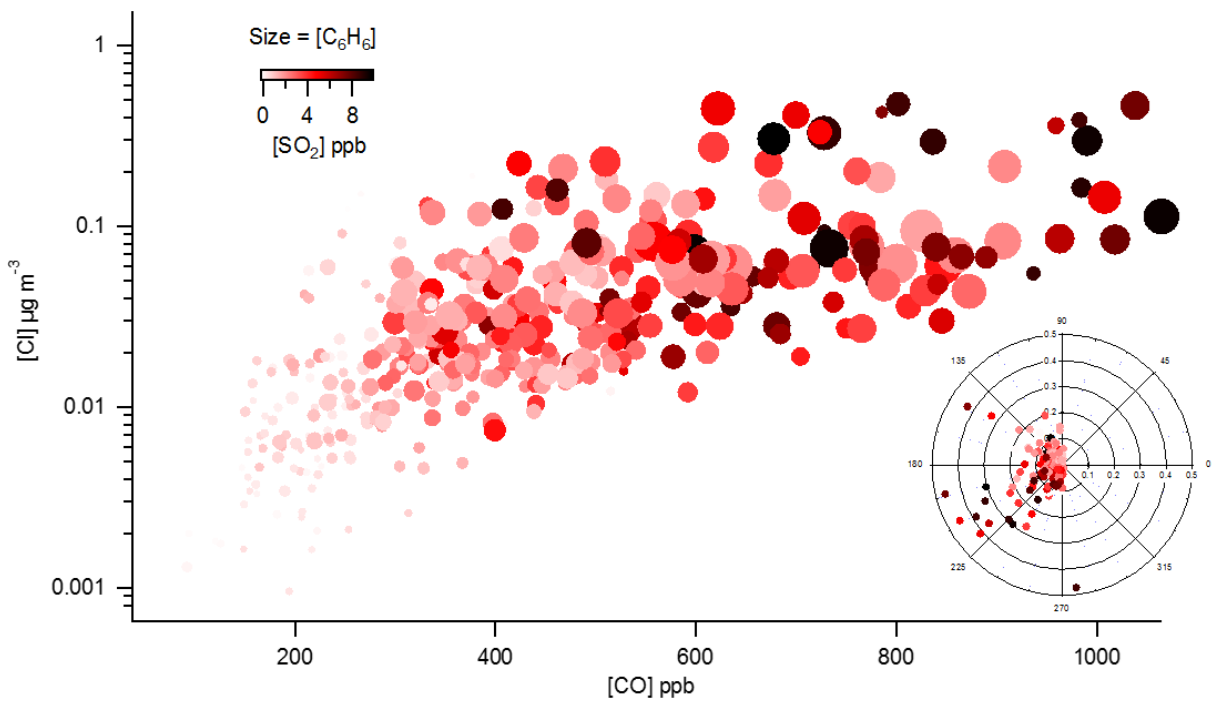
7



1

2 **Figure 3. Mean diurnal profiles of the inorganic halogens detected by the CIMS from the 23<sup>rd</sup> May to 6<sup>th</sup>**  
 3 **June with average J rate for ClNO<sub>2</sub> as guide for photolysis. ClNO<sub>2</sub> and HCl mixing ratios are on the left y-**  
 4 **axis and the other inorganic halogens on the right y-axis**

5

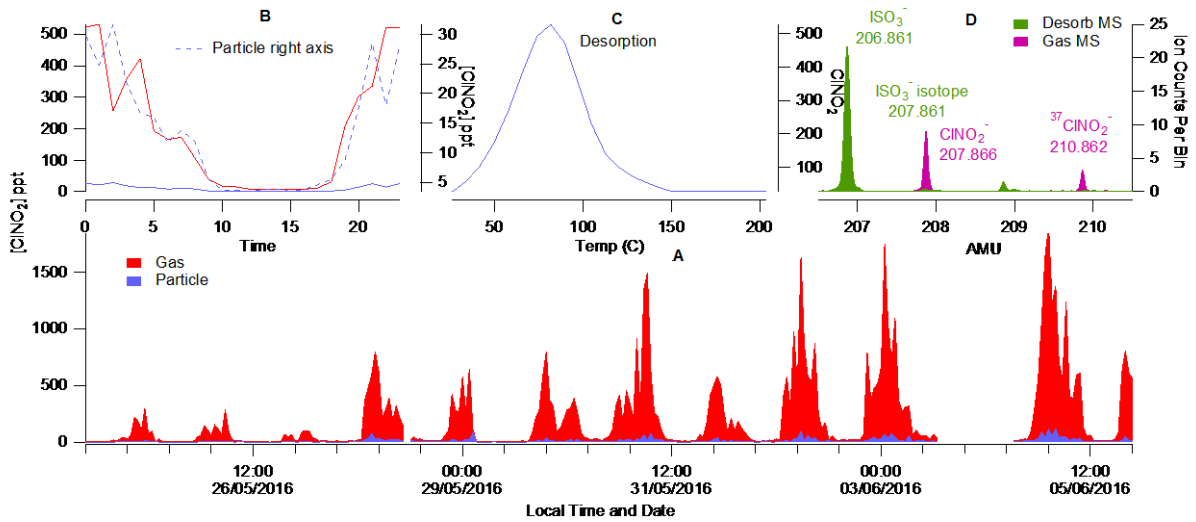


6



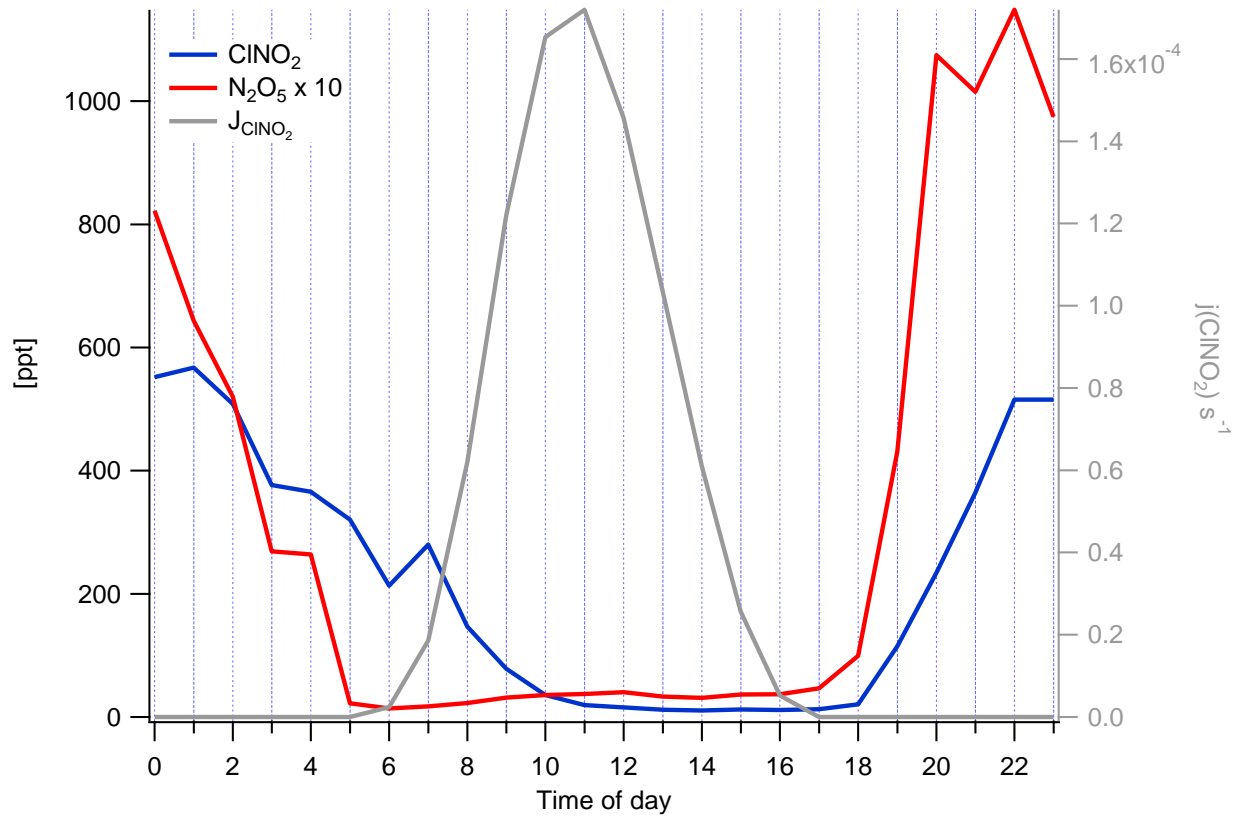
1 **Figure 4. Correlation of particulate Cl<sup>-</sup> from the AMS measurements and CO colour coded by SO<sub>2</sub> mixing**  
 2 **ratio and size binned by increasing benzene mixing ratio. A wind rose plot illustrates the wind direction and**  
 3 **particulate Cl<sup>-</sup> mixing ratio colour coded by SO<sub>2</sub> mixing ratio.**

4  
5  
6



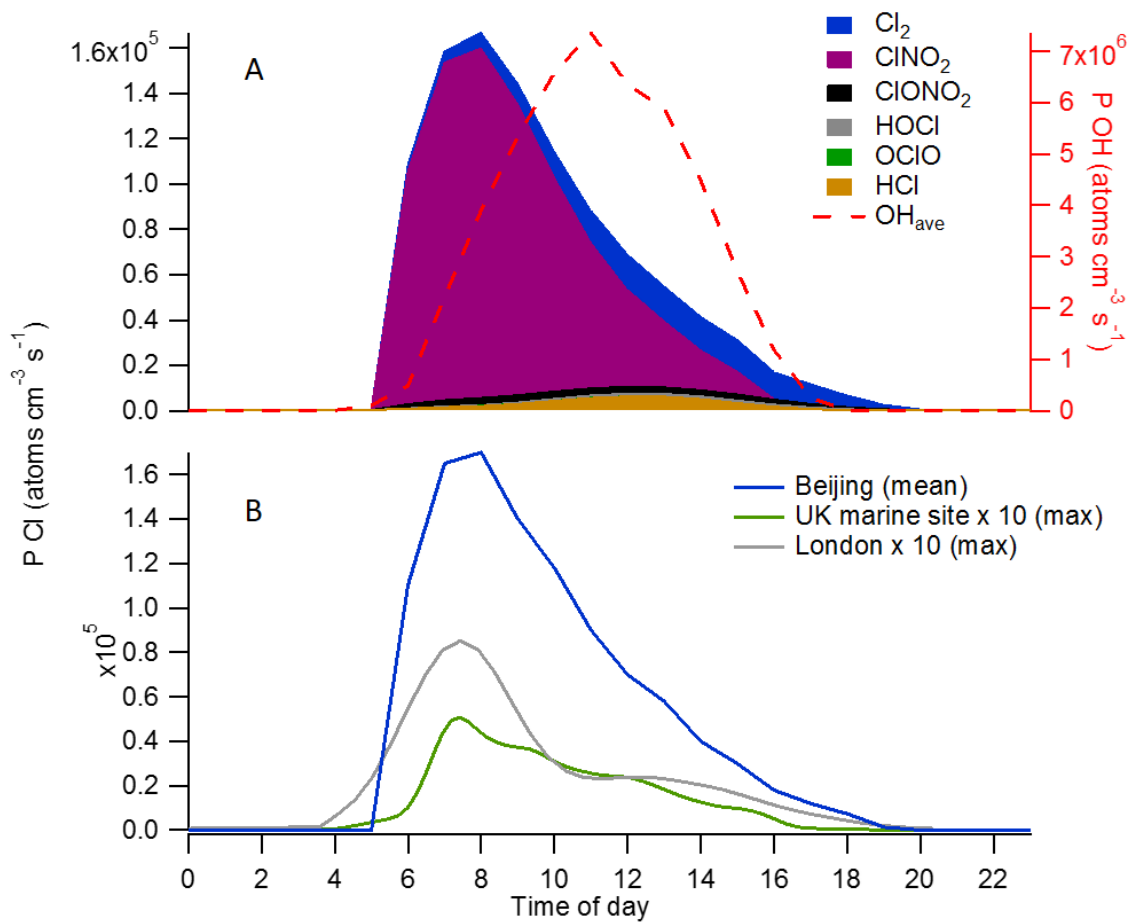
7  
8  
9  
10  
11

8 **Figure 5. CINO<sub>2</sub> gas and particle phase campaign time series (1 hour averaged) (panel A) and average**  
 9 **diurnal profiles Panel B). The peak fitting for CINO<sub>2</sub> and the SO<sub>3</sub> interfering mass at 207-208 AMU (panel**  
 10 **C) and the desorption profile for the counts attributed to the high resolution CINO<sub>2</sub> peak (panel D).**



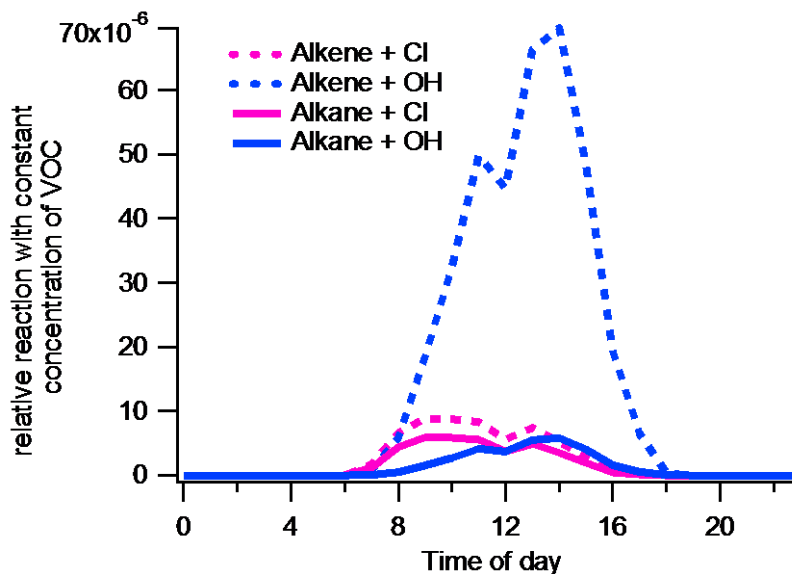
1

2 **Figure 6. Diurnal profile of  $\text{N}_2\text{O}_5$ ,  $\text{ClNO}_2$  and  $j(\text{ClNO}_2)$  for the campaign highlighting the persistence of**  
 3  **$\text{ClNO}_2$  passed sunrise and the expected rapid photolysis of  $\text{N}_2\text{O}_5$ .**



1

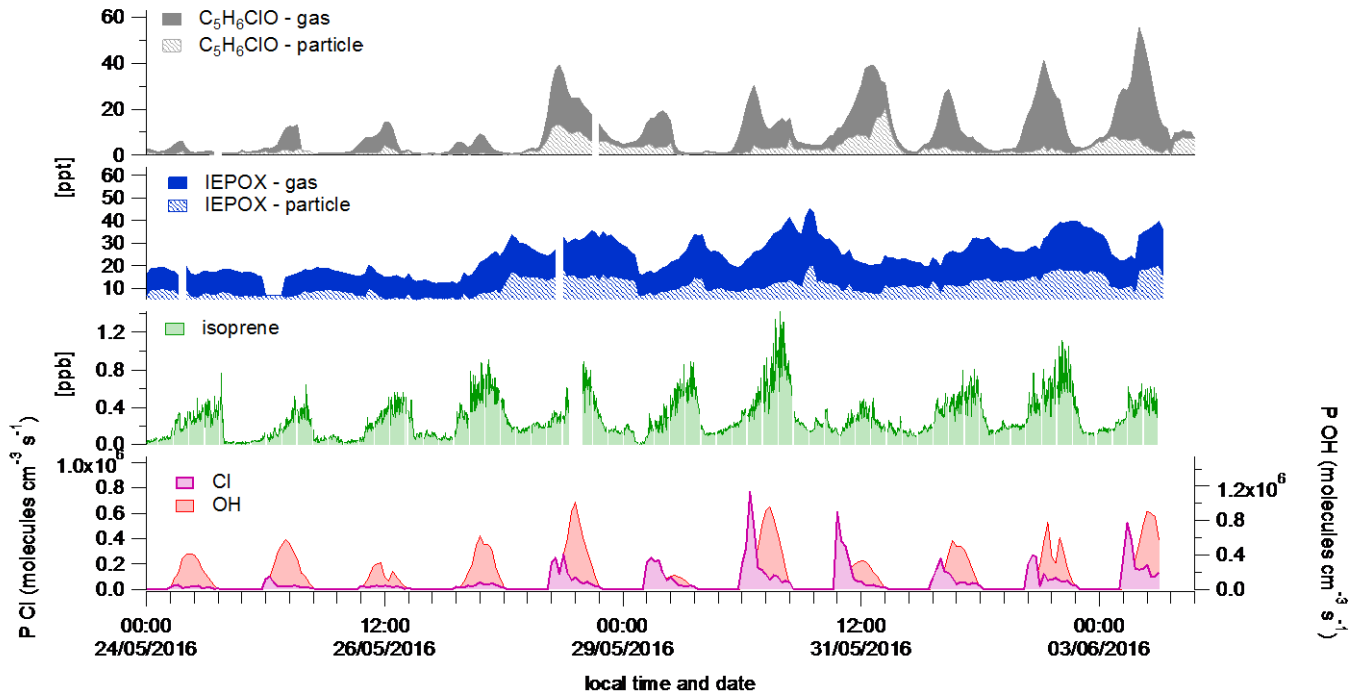
2 **Figure 7. A) Steady state calculation of inorganic halogens contribution to chlorine atom production. B)**  
 3 **Relative mean diurnal profiles of calculated chlorine atom mixing ratio calculation from this work (Beijing)**  
 4 **and measurements in the UK (London (Bannan et al., 2015) and a marine site (Weybourne Atmospheric**  
 5 **Observatory-Bannan et al., (2017)). The steady state OH production rate from Beijing is also displayed to**  
 6 **illustrate relative mixing ratios of oxidants.**



7

1 **Figure 8. Mean diurnal time series of alkene (pink) and alkane (blue) relative reaction rate (arbitrary value)**  
 2 **with the chlorine atom (dashed) and OH (solid).**

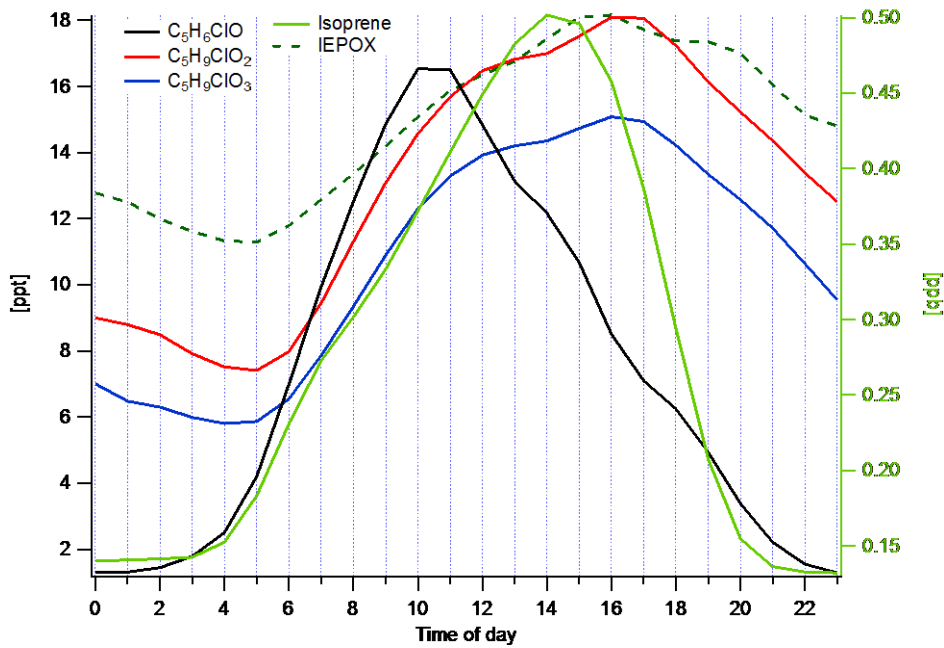
3



4

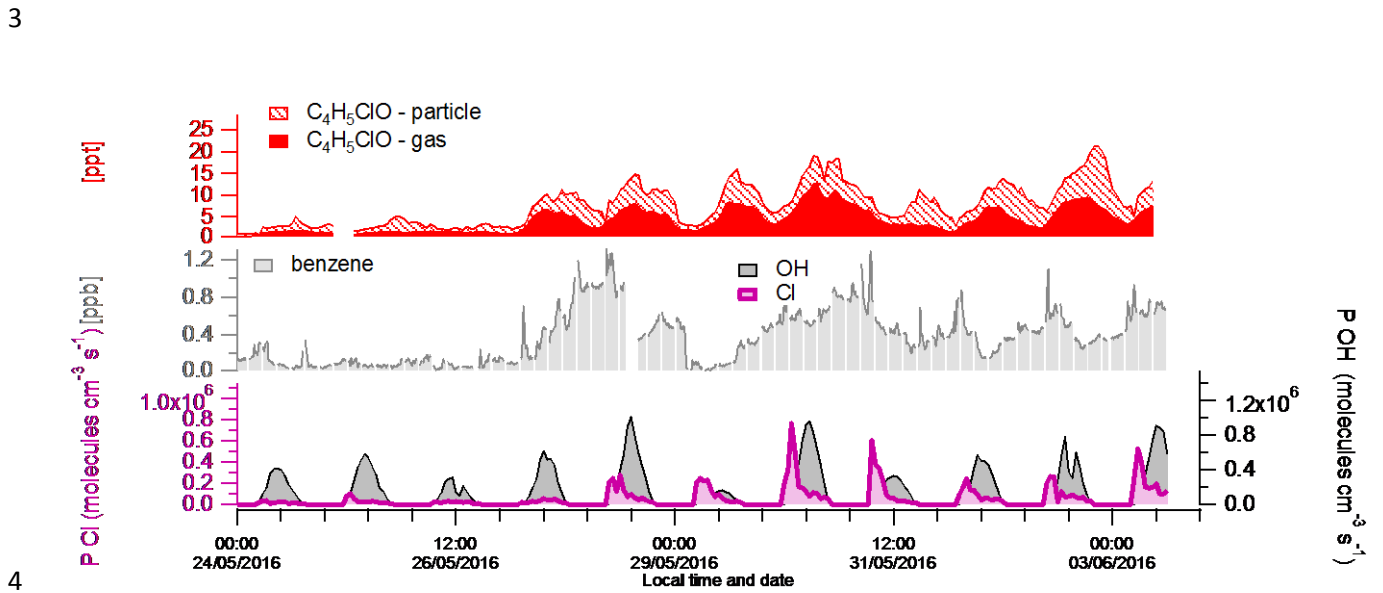
5 **Figure 9. Campaign time series of isoprene, IEPOX, CMBO and steady state production rate of chlorine**  
 6 **atoms and OH**

7

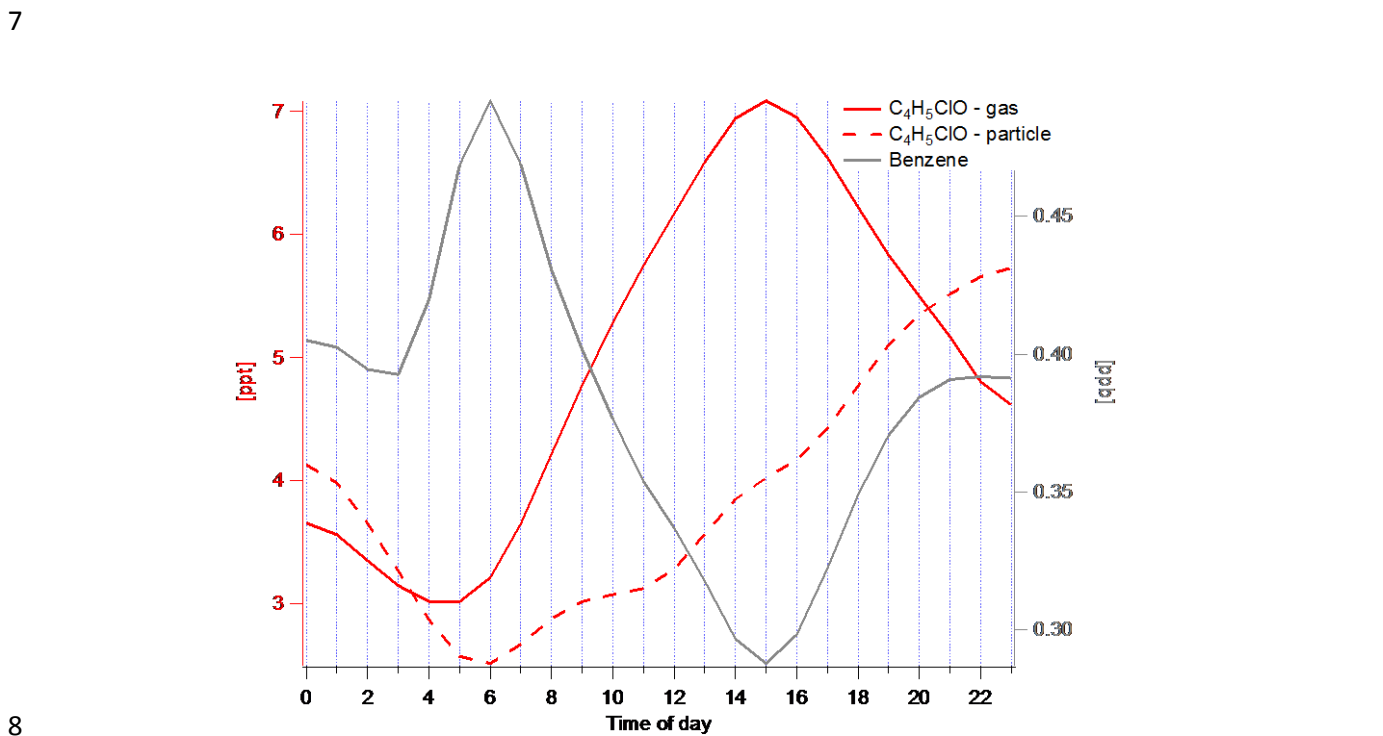


8

1 Figure 10. Mean diurnal profiles of isoprene (right y-axis) and its OH oxidation product (IEPOX) and  
 2 chlorine atom oxidation products CMBO,  $C_5H_9ClO_2$  and  $C_5H_9ClO_3$  (left y-axis



5 Figure 11. Campaign time series of benzene and CCA with supporting calculations of OH and the chlorine  
 6 atom production rates



9 Figure 12. Mean campaign diurnal profiles of benzene (grey) and CCA in the particle (dashed red) and gas  
 10 phase (solid red).

11